

UC Berkeley

UC Berkeley Previously Published Works

Title

Covalent targeting of the vacuolar H<sup>+</sup>-ATPase activates autophagy via mTORC1 inhibition

Permalink

<https://escholarship.org/uc/item/04p7r2rg>

Journal

Nature Chemical Biology, 15(8)

ISSN

1552-4450

Authors

Chung, Clive Yik-Sham

Shin, Hijai R

Berdan, Charles A

et al.

Publication Date

2019-08-01

DOI

10.1038/s41589-019-0308-4

Peer reviewed



# HHS Public Access

Author manuscript

*Nat Chem Biol.* Author manuscript; available in PMC 2020 January 08.

Published in final edited form as:

*Nat Chem Biol.* 2019 August ; 15(8): 776–785. doi:10.1038/s41589-019-0308-4.

## Covalent Targeting of the Vacuolar H<sup>+</sup>-ATPase Activates Autophagy Via mTORC1 Inhibition

Clive Yik-Sham Chung<sup>1,2,\*</sup>, Hijai R. Shin<sup>3,5,\*</sup>, Charles A. Berdan<sup>4</sup>, Breanna Ford<sup>4</sup>, Carl C. Ward<sup>2,3</sup>, James A. Olzmann<sup>4</sup>, Roberto Zoncu<sup>3,5,#</sup>, and Daniel K. Nomura<sup>1,2,3,4,#</sup>

<sup>1</sup>Department of Chemistry, University of California, Berkeley, Berkeley, CA 94720, USA

<sup>2</sup>Novartis-Berkeley Center for Proteomics and Chemistry Technologies

<sup>3</sup>Department of Molecular and Cell Biology, University of California, Berkeley, Berkeley, CA 94720, USA

<sup>4</sup>Department of Nutritional Sciences and Toxicology, University of California, Berkeley 94720, USA

<sup>5</sup>The Paul F. Glenn Center for Aging Research at the University of California, Berkeley, Berkeley, CA 94720, USA

### Abstract

Autophagy is a lysosomal degradation pathway that eliminates aggregated proteins and damaged organelles to maintain cellular homeostasis. A major route for activating autophagy involves inhibition of the mTORC1 kinase, but current mTORC1-targeting compounds do not allow complete and selective mTORC1 blockade. Here, we have coupled screening of a covalent ligand library with activity-based protein profiling to discover EN6, a small-molecule *in vivo* activator of autophagy that covalently targets cysteine 277 in the ATP6V1A subunit of the lysosomal v-ATPase, which activates mTORC1 via the Rag guanosine triphosphatases. EN6-mediated ATP6V1A modification decouples the v-ATPase from the Rags, leading to inhibition of mTORC1 signaling, increased lysosomal acidification, and activation of autophagy. Consistently, EN6 clears TDP-43 aggregates, a causative agent in frontotemporal dementia, in a lysosome-dependent manner. Our results provide insight into how the v-ATPase regulates mTORC1, and reveal a unique approach for enhancing cellular clearance based on covalent inhibition of lysosomal mTORC1 signaling.

### Editorial Summary

Users may view, print, copy, and download text and data-mine the content in such documents, for the purposes of academic research, subject always to the full Conditions of use:[http://www.nature.com/authors/editorial\\_policies/license.html#terms](http://www.nature.com/authors/editorial_policies/license.html#terms)

#correspondence to rzoncu@berkeley.edu and dnomura@berkeley.edu.

Author Contributions

CYSC, HRS, RZ, DKN conceived the project and wrote the paper. CYSC, HRS, CAB, BF, RZ, DKN designed and performed the experiments. CYSC, HRS, CAB, CCW, RZ, DKN analyzed data. JAO provided reagents.

\*these authors contributed equally to this work

Data Availability Statement

The datasets generated during and/or analyzed during the current study are available from the corresponding authors on reasonable request.

We report here a covalent ligand that targets C277 of ATP6V1A leading to enhanced v-ATPase activity, inhibition of mTORC1 signaling, increased lysosomal acidification, activation of autophagy, and clearance of toxic protein aggregates.

## Keywords

autophagy; chemoproteomics; activity-based protein profiling; cysteine; covalent ligand; mTORC1; v-ATPase; lysosome; ATP6V1A

## Introduction

Autophagy is central to the maintenance of organismal homeostasis in both physiological and pathological situations. It is an essential, conserved lysosomal degradation pathway that controls the quality of the cytoplasm by eliminating aggregated proteins and damaged organelles. Accordingly, alterations in autophagy have been linked to a wide range of diseases and conditions, including aging, cancer, metabolic disorders, and neurodegenerative diseases<sup>1,2</sup>. Throughout the past decade, autophagy has attracted considerable attention as a target for the development of novel therapeutics<sup>3,4</sup>.

The activity of the autophagic machinery is tightly linked to upstream signals from nutrients, energy and stressors through the mechanistic target of rapamycin complex 1 (mTORC1) protein kinase. mTORC1 phosphorylates and inhibits a master switch for autophagosome formation, the ULK1 kinase along with its accessory factor Atg13<sup>5,6</sup>. Moreover, mTORC1 blocks the nuclear translocation and activation of the MiT/TFE family transcription factor TFEB which, along with closely related TFE3, functions as a ‘master regulator’ of catabolism by coordinately promoting the expression of genes required for autophagosome formation and lysosomal function<sup>5-7</sup>. Inhibition of mTORC1 resulting from starvation or chemical inhibitors triggers autophagy by simultaneously unleashing the activity of ULK1 and TFEB. Thus, chemical inhibition of mTORC1 is viewed as a prime strategy for activating autophagy in physiological settings.

Most protein misfolding diseases are associated with intracytoplasmic deposition of aggregate-prone proteins in neurons and non-neuronal cells, which impair essential cellular pathways for transport, energy production and quality control<sup>8</sup>. Over recent years, evidence has accumulated to demonstrate that upregulation of autophagy is protective against neurodegeneration. In particular, aggregate-prone proteins that drive the toxicity of Huntington’s disease (HD), Amyotrophic Lateral Sclerosis (ALS) and Fronto-Temporal Dementia (FTD) among others are autophagic substrates, and pharmacological activators of autophagy can be beneficial in both cell and animal models of these diseases, by both degrading intracytoplasmic aggregates and by preventing associated cell death<sup>9-11</sup>.

While several autophagy-modulating agents have been discovered, many of these compounds do not possess the required specificity to activate autophagy in a safe manner, either due to off-target effects or due to multiple functions of their target protein. The allosteric mTORC1 inhibitor, rapamycin, results in the relatively specific inhibition of mTORC1 by causing its binding to FK506-binding protein 1A (FKBP1A). However,

rapamycin is an incomplete mTORC1 inhibitor; most notably it largely fails at blocking mTORC1-dependent inhibitory phosphorylation of ULK1 and TFEB and at triggering their pro-catabolic programs. Thus, despite some early success *in vitro*, rapamycin-based drugs (Rapalogues) have proven ineffective in reducing neurotoxic protein aggregates<sup>12,13</sup>. The recently developed ‘ATP-competitive’ compounds block the kinase activity of mTOR toward virtually all substrates. The higher potency and broader range of ATP-competitive mTOR inhibitors has led to promising results in cancer clinical trials; however, these compounds have shown considerable side-effects and the ability to cause substantial toxicity to pancreatic  $\beta$ -cell islets leading to  $\beta$ -cell death. Most relevant in the context of neurodegenerative disease, ATP competitive mTOR inhibitors strongly suppress Akt signaling, which is an essential survival signal for neuronal cells<sup>14–16</sup>. The limitations of current mTOR inhibitors thus create an urgent need to identify new targets that could lead to activation of autophagy while avoiding unacceptable toxicities.

To be activated, mTORC1 needs to translocate to the lysosome membrane<sup>5,6</sup>. Nutrients, including amino acids, glucose and cholesterol, regulate the lysosomal recruitment of mTORC1 by modulating the nucleotide state of the Rag GTPases<sup>17–19</sup>. The Rags assemble as obligate heterodimers composed of RagA or RagB (which are highly similar to each other) associated with RagC or RagD, and are tethered to the lysosomal membrane by the pentameric Ragulator complex, composed of the LAMTOR1–5 proteins<sup>17,20,21</sup>. Under amino acid sufficiency, the Rag GTPases become active by adopting a nucleotide state in which Rag-A/B is GTP-loaded and Rag-C/D is GDP-loaded, and mediate the lysosomal attachment of mTORC1 by directly interacting with the mTORC1 subunit Raptor<sup>17,20,21</sup>.

A key but poorly understood player in Rag-mTORC1 activation is the vacuolar H<sup>+</sup> ATPase (v-ATPase), an evolutionarily conserved ATP-driven rotary proton pump that couples ATP hydrolysis by its peripheral V1 domain to proton translocation through membrane integral V0 domain to acidify the lysosome and enable its degradative functions<sup>22,23</sup>. The v-ATPase forms a physical supercomplex with Ragulator and the Rag GTPases, and its integrity and activity are essential for lysosomal mTORC1 recruitment in response to amino acids<sup>18,24–26</sup>. Although its precise role in Rag-mTORC1 activation is not completely understood, the v-ATPase represents a prime target for discovery of small molecules that may simultaneously block mTORC1 activation and enhance autophagic function. In this study, through the coupling of chemoproteomics and covalent ligand screening, we have discovered a small-molecule activator of autophagy that acts through covalent targeting of a unique regulatory cysteine on ATP6V1A, resulting in the complete inactivation of mTORC1 without affecting off-target Akt signaling pathways, and enhanced cellular clearance of toxic protein aggregates.

## Results

### Covalent Screen Reveals EN6 as an Autophagy Activator

To simultaneously discover new targets, druggable hotspots and small-molecule modulators for activating autophagy, we screened a library of 217 cysteine- and lysine-reactive ligands based on acrylamide, chloroacetamide, and dichlorotriazine scaffolds in a cell-based autophagic flux assay that utilizes a dual-color, cleavable LC3B reporter<sup>27–30</sup>. By running

this screen in mouse embryonic fibroblast (MEF) cells, we identified several covalent ligands that increased LC3B processing and thus potentially increased autophagy activation (Supplementary Fig. 1a, Supplementary Tables 1–4, Supplementary Dataset 1). mTORC1 inhibitors rapamycin and Torin1 also demonstrated expected efficacy in this assay. Upon replication in human HEK293A cells, the screen yielded the cysteine-reactive acrylamide EN6 (**1**) as an inducer of LC3B degradation to a comparable degree to direct mTORC1 inhibitors, rapamycin and Torin1 (Fig. 1a–1c). We validated these findings by showing that, in HEK293A cells, EN6 treatment increased the levels of processed LC3BII (Fig. 1d), and triggered formation of LC3 puncta to a similar degree to Torin1 treatment in a time- and dose-dependent manner (Fig. 1e; Supplementary Fig. 1b–S1d). EN6 treatment in HEK293A cells also led to significant increases in the number autophagosomes and autolysosomes (Supplementary Fig. 1e–1f).

### Chemoproteomics Identifies v-ATPase as an EN6 Target

To discover the mechanism of action of EN6, we next mapped its proteome-wide cysteine-reactivity in MEF cells using competitive isotopic tandem orthogonal proteolysis-enabled activity-based protein profiling (isoTOP-ABPP) (Supplementary Fig. 2a, Fig. 2a, Supplementary Dataset 2). Upon *in situ* treatment of cells with vehicle or EN6, we labeled the resulting cell lysates with the cysteine-reactive alkyne-functionalized iodoacetamide probe (IA-alkyne) followed by the isoTOP-ABPP chemoproteomics pipeline<sup>31–33</sup>. The primary labeling site of EN6 was identified as cysteine 277 (C277) of ATP6V1A, the catalytic subunit of the lysosomal v-ATPase (Fig. 2a). This site showed an isotopic light-to-heavy (control-to-EN6-treated) ratio of 6.3, indicating target engagement of this site compared to other sites. We confirmed this interaction by demonstrating that EN6 displaced tetramethylrhodamine-5-iodoacetamide dihydroiodide (IA-rhodamine) labeling from recombinant human ATP6V1A protein with an IC<sub>50</sub> of 1.7 μM (Fig. 2b). The incomplete inhibition of IA-rhodamine labeling by EN6 likely indicates reactivity of the IA-rhodamine probe with other ligandable sites within ATP6V1A that are not engaged by EN6<sup>34</sup>.

### EN6 Blocks mTORC1 Lysosomal Localization and Activation

Previous studies have shown that the lysosomal v-ATPase physically interacts with the Ragulator-Rag complex and enables it to recruit mTORC1, leading to activation of mTORC1-dependent anabolic programs and inhibition of autophagy initiation<sup>18,26</sup>. We thus asked whether, by binding to the ATP6V1A subunit of the v-ATPase, EN6 may disrupt mTORC1 recruitment to the lysosome, thus leading to its observed autophagy-activating effects. Consistent with this premise, we found that EN6 treatment in cells led to complete inactivation of mTORC1 signaling, as shown by reduced levels of phosphorylated canonical substrates, S6 kinase 1 (S6K1), 4EBP1, and ULK1, in a dose-responsive and time-dependent manner (Fig. 2c, Supplementary Fig. 2b–2c). Notably, consistent with specific involvement of the v-ATPase in mTORC1 but not mTORC2 regulation, treatment with EN6 had no effect on mTORC2-dependent AKT phosphorylation, whereas the ATP-competitive mTOR inhibitor, Torin1, blocked AKT phosphorylation completely (Fig. 2c, Supplementary Fig. 2d).

Confirming that mTORC1 inhibition by EN6 involves modification of C277 of ATP6V1A, phosphorylation of S6K and ULK1 were completely resistant to EN6-mediated inhibition in cells in which endogenous ATP6V1A was knocked down and replaced with the non-modifiable C277A or C277S mutants (Fig. 2d, Supplementary Fig. 2e, 2f and 2g). Mutation of C277 to an alanine or serine did not affect v-ATPase activity or its sensitivity to the v-ATPase inhibitor bafilomycin A1 (BafA1), as shown in a lysosomal re-acidification assay *in vitro* that monitors v-ATPase-dependent quenching of pH-sensitive FITC-conjugated dextran<sup>18,35</sup> (Supplementary Fig. 2g). In these cells, EN6-induced LC3BII accumulation and p62/SQSTM1 degradation were also prevented by the C277A and C277S substitutions, indicating that autophagy activation by EN6 is also strictly dependent on C277 modification (Fig. 2d, Supplementary Fig. 2h). To further demonstrate that the activity of EN6 is driven by covalent modification by the acrylamide cysteine-reactive warhead, we showed that treatment of HEK293A cells with a cysteine non-reactive analog of EN6, CC2-49 (2), did not inhibit mTORC1 signaling or elevate LC3BII levels (Supplementary Fig. 2i–2j).

The v-ATPase interacts with Ragulator-Rags to enable GTP loading of RagA/B, leading to recruitment of mTORC1 to the lysosome<sup>18,26</sup>. Consistent with an inhibitory mechanism towards this pathway, EN6 was completely ineffective at blocking mTORC1 signaling in cells either expressing a constitutively active, GTP-locked RagB<sup>Q99L</sup> mutant protein, or in cells with knockout of the GATOR1 complex protein NPRL3, which promotes GTP hydrolysis of RagA/B to inactivate them (Fig. 3a–3b)<sup>36</sup>. Further supporting an inhibitory action via the Rag GTPases, EN6 treatment completely abrogated amino acid-induced mTORC1 recruitment to LAMP2-positive lysosomes, and this effect was prevented by exogenously expressing the GTP-locked RagB<sup>Q99L</sup> mutant protein (Fig. 3c–3d; Supplementary Fig. 3).

Although how the v-ATPase promotes GTP loading of RagA/B is not understood, its action involves physical interaction with the Ragulator-Rags complex that is modulated by amino acids<sup>18,26</sup>. Consistently, FLAG-tagged Ragulator subunit p14 immunoprecipitated multiple v-ATPase subunits in an amino acid-regulated manner (Fig. 3e). Notably, EN6 decreased the overall binding between the v-ATPase and Ragulator and rendered this interaction insensitive to amino acids (Fig. 3e). The most parsimonious explanation for this result is that covalent modification of C277 of ATP6V1A by EN6 causes a conformational change in the v-ATPase that partially decouples it from Ragulator-Rag and prevents activation of the latter complex by amino acids. Collectively, these data reveal that, by targeting C277 of ATP6V1A, EN6 impairs Rag GTPase-mediated recruitment of mTORC1 to the lysosome, leading to starvation-independent induction of autophagy.

### EN6 Activates the v-ATPase and Lysosome Acidification

mTORC1 inhibition leads to upregulation of the catabolic functions of the lysosome through dephosphorylation and nuclear translocation of TFEB<sup>5,7,37,38</sup>. Consistently, upon EN6 treatment we observed greatly enhanced TFEB nuclear translocation (Fig. 4a, Supplementary Fig. 4a) and significantly increased levels of several lysosomal gene transcripts that are direct TFEB transcriptional targets, including v-ATPase components (Fig.

4b, Supplementary Fig. 4b). In contrast, the expression levels of several genes that are not TFEB targets were unchanged (Supplementary Fig. 4c).

Consistent with transcriptional upregulation of the v-ATPase and other lysosomal components, EN6 treatment led to significantly increased acidification of the lysosome in HEK293A cells, as shown by ratiometric LysoSensor DND-160 staining, and this heightened acidification was blocked by BafA1 (Fig. 4c, 4d; Supplementary Fig. 4d). Intriguingly, while BafA1 expectedly inhibited *in vitro* v-ATPase activity, EN6 treatment increased the catalytic activity of the v-ATPase, as shown by accelerated acidification of FITC-dextran-loaded lysosomes *in vitro* (Fig. 4e). Thus, the increased lysosomal acidification observed with EN6 is likely due to a combination of increased expression of v-ATPase catalytic subunits and direct stimulation of v-ATPase catalytic activity.

### EN6 Promotes Autophagic Clearance of Protein Aggregates

To determine whether EN6-mediated inhibition of mTORC1 and activation of autophagy could aid in boosting cellular clearance, we tested the effect of EN6 in clearing toxic Tar-binding protein 43 (TDP43) protein aggregates, which drive the pathogenesis of amyotrophic lateral sclerosis (ALS)<sup>39</sup>. In an IPTG-inducible GFP-TDP43 U2OS osteosarcoma cell line model, IPTG stimulation led to the rapid formation of TDP43 aggregates, which were reduced by 75 % upon 7 hours of EN6 cotreatment (Fig. 4f, Supplementary Fig. 4e). EN6-mediated clearance of TDP43 aggregates was lysosome- and v-ATPase-dependent, as it was prevented by co-treatment with BafA1 (Fig. 4f, Supplementary Fig. 4e). We observed pronounced clearance of TDP43 aggregates in IPTG pre-stimulated cells within as little as 4 hours of EN6 treatment, suggesting that the post-transcriptional actions of EN6 are sufficient to boost cellular clearance (Supplementary Fig. 4f–4i).

A previous study reported a covalent ligand, that we name CZ (3) here (Supplementary Fig. 5a), that targets an alternate C138 in human ATP6V1A that reportedly inhibits v-ATPase activity<sup>34</sup>. We verified that CZ significantly inhibited v-ATPase activity *in vitro* and in cells, albeit to a lesser extent than BafA1, whereas EN6 stimulated v-ATPase activity (Supplementary Fig. 5b–5c). Consistent with v-ATPase inhibition and similarly to BafA, CZ inhibited LC3b processing and p62 degradation, whereas EN6 stimulated it (Supplementary Fig. Fig. 5d–5e). CZ also did not clear TDP43 aggregates (Supplementary Fig. 5f). v-ATPase inhibition by BafA was previously shown to inhibit mTORC1 and, similarly, CZ treatment decreased mTORC1 signaling, as did EN6 (Supplementary Fig. 5g)<sup>18</sup>. However, consistent with a different mechanism of action, CZ did not alter mTORC1 lysosomal localization under amino acid stimulation, whereas EN6 effectively abolished it (Supplementary Fig. 5h–5i)<sup>34</sup>. Taken together these data demonstrate that, by covalently targeting different cysteines within ATP6V1A, EN6 and CZ exert profoundly different actions, whereby only EN6 has the desired profile of simultaneous mTORC1 inhibition and v-ATPase activation that dramatically boosts cellular clearance.

## EN6 Inhibits mTORC1 and Activates Autophagy In Vivo

We next tested whether EN6 was able to inhibit mTORC1 and activate autophagy *in vivo*. Previous studies have shown that inhibition of mTORC1 signaling improves cardiac and skeletal muscle in various disease paradigms, including muscular dystrophy, cardiomyopathy, aging, and sarcopenia<sup>40–43</sup>. We thus focused our attention on mTORC1 signaling and autophagy in skeletal muscle and heart. Dose-response and time-course studies showed bioavailability of EN6 in skeletal muscle and heart within one hour of treating mice with 50 mg/kg intraperitoneal (i.p.) dose (Supplementary Fig. 6a). EN6 treatment significantly inhibited mTORC1 signaling in both skeletal muscle and heart, as demonstrated by reduced phosphorylation of S6, 4EBP1, and ULK1 whereas autophagy was strongly activated, as shown by heightened LC3BII levels and reduced p62 levels (Fig. 5a–5b, Supplementary Fig. 6b). While EN6 was somewhat less potent than rapamycin in shutting down p-S6, it was significantly more effective than rapamycin at inhibiting phosphorylation of 4EBP1 and ULK1, as well as inducing LC3b cleavage and p62 degradation, consistent with our data in cell lines (Fig. 5a–5b). We also did not observe inhibition of mTORC2-dependent AKT phosphorylation with EN6 treatment (Fig. 5a–5b, Supplementary Fig. 6b). While we only tested EN6 effects upon mTORC1 signaling and autophagy in skeletal muscle and heart in this study, it will be of future interest to determine the effects of EN6 in additional tissues. Thus, due to its unique mechanism of action, EN6 functions as a complete mTORC1 inhibitor without affecting off-target AKT signaling pathways, and induces autophagy and lysosomal degradation both in cells and *in vivo*.

## Discussion

Our study identifies a covalent ligand, EN6, which targets a unique druggable hotspot—C277 within the  $\nu$ -ATPase subunit ATP6V1A—to activate autophagy by completely inhibiting mTORC1 signaling through disrupting mTORC1 localization to the lysosome without affecting off-target AKT signaling pathways (Fig. 6). This is a distinct mechanism from other pharmacological modulators of autophagy such as with rapalogues and ATP-competitive inhibitors, which act through directly targeting the kinase function mTORC1. While both rapalogues and ATP-competitive mTORC1 inhibitors have potential therapeutic activity, their clinical utility is hampered by their incomplete mTORC1 inhibition (rapalogues) and concomitant inhibition of mTORC2 (ATP competitors)<sup>44–46</sup>. Chronic exposure to rapalogues also inhibits mTORC2, leading to metabolic dysregulation<sup>47,48</sup>. Whereas the effects of long-term EN6 treatment on mTORC2 signaling remain to be determined, the ability of EN6 to selectively target an mTORC1-specific activation node makes it unlikely that mTORC2 inhibition will occur (Refs 6, 47, 48 here). EN6 shows promising cellular and *in vivo* activity. However, this covalent ligand is an early hit that still requires further medicinal chemistry efforts to optimize potency, selectivity, *in vivo* bioavailability and efficacy, and ideally brain penetrance. While we show here that EN6 inhibits mTORC1 signaling after 4 h of treatment in mice, we do not yet know how long this inhibition is sustained *in vivo*. Since EN6 is irreversibly bound to ATP6V1A, the reactivation of ATP6V1A will likely depend on protein turnover rates. Furthermore, while isoTOP-ABPP studies here show that C277 of ATP6V1A is one of the primary and most highly engaged targets of EN6 in cells, EN6 may possess additional off-targets that either



exhibit lower degree of engagement, react with other amino acids, or act through reversible interactions that may contribute to EN6 effects on autophagy or trigger additional biological effects that need to be determined. Development of an alkyne-functionalized EN6 probe will aid in future assessment of EN6 selectivity and provide a foundation for additional medicinal chemistry, target engagement, and screening efforts to identify improved ligands against this site. Nonetheless, our study convincingly demonstrates that the EN6 effects upon mTORC1 signaling and autophagy are driven through the targeting of C277 of ATP6V1A.

A key question is how covalent modification of C277 within ATP6V1A affects v-ATPase function and mTORC1 regulation. By inspecting the previously reported crystal structures of the v-ATPase from *Thermus Thermophilus* and *Enterococcus Hirae*<sup>49</sup>, we note that the equivalent residues to human C277, C255 in *Thermus* and C259 in *Enterococcus* V1A subunits, respectively, lie in the core of the catalytic B-A interface, in close proximity to residues that are critical for catalysis, such as E279 in human (E257 in *Thermus* and E261 in *Enterococcus*, respectively). Because the side chain of C277 points away from the nucleotide, this residue is unlikely to directly participate in catalysis. However, covalent modification of this cysteine likely results in realignment of nearby residues, leading to higher rate of ATP hydrolysis and/or increased coupling between the V1 and V0 domains that ultimately accelerates proton pumping and lysosomal acidification<sup>50</sup>.

Is the increased v-ATPase catalytic rate related to the observed strong inhibition of mTORC1 signaling by EN6? A plausible model supported by previous data is that a fraction of the energy generated by ATP hydrolysis may be utilized for mTORC1 activation via the physical coupling between the v-ATPase and Ragulator-Rags (Fig. 6)<sup>18</sup>. Consistent with this model, our co-IP data indicate that the conformational change induced by covalent modification of C277 partially uncouples the v-ATPase from Ragulator-Rag, making their binding insensitive to amino acids and weaker overall.

The physical coupling model proposed here is not in conflict with previous studies where blocking the v-ATPase using ConA or BafA results in mTORC1 inhibition<sup>18,26</sup>. According to this model, mTORC1 activation can be prevented by either BafA-mediated inhibition of the v-ATPase catalytic function (such that no energy is generated for Rag regulation) or by making this energy unavailable through disrupted interaction between v-ATPase and Ragulator-Rags (as in the case of EN6). Future structural biology efforts on reconstituted v-ATPase-Ragulator-Rag supercomplex will yield additional insights into the mechanism through which the v-ATPase enables mTORC1 recruitment to the lysosome, and into how covalent modification by EN6 disrupts this process.

A major challenge of chemical genetic screens is identifying the targets of leads that arise from screens. The structures lead compounds must often be altered or derivatized to bear biorthogonal and photoaffinity handles or conjugated to beads to facilitate chemoproteomic target identification. These approaches require additional synthetic efforts to make analogs of the lead molecule and alter the structure of the molecule, which may hinder or prevent initial target identification efforts. Previous studies have highlighted the utility of covalent ligands and ABPP-based approaches in accessing unique ligandable sites within classically

undruggable protein targets<sup>31,33</sup>. Our study once again highlights the utility of chemoproteomics-enabled covalent ligand screening platforms to rapidly deconvolute the mechanism of action of cellular phenotypic screening hits and uncover unique and novel ligandable sites and druggable modalities that would not be predicted *a priori*. In this study, we reveal a cell and *in vivo*-active covalent ligand EN6 that uniquely targets a novel ligandable cysteine within the ATP6V1A component of the v-ATPase complex to inhibit mTORC1 signaling and activate autophagy to improve cellular clearance.

## Online Methods

### Cell Culture

Human embryonic kidney HEK293T and HEK293A cells, mouse embryonic fibroblasts (MEF), HeLa cells, HEK293A cells stably expressing GFP-LC3-RFP-LC3 G (plasmid purchased from Addgene), MEF cells stably expressing GFP-LC3-RFP-LC3 G (plasmid purchased from Addgene) and human bone osteosarcoma epithelial U2OS cells stably expressing an IPTG-inducible GFP-TDP43 were maintained in DMEM supplemented with 10 vol% FBS and 1 vol% GlutaMax. GFP-TDP43 cell lines were purchased from Innoprot (P30710). All cells were incubated in 5% CO<sub>2</sub> humidified air, and subcultured when 80% confluence was reached. They were free of mycoplasma contamination, and routinely checked using MycoAlert Mycoplasma Detection Kit (Lonza, LT07–318) and DAPI staining.

### Screening for autophagy modulators

MEF cells stably expressing GFP-LC3-RFP-LC3 G were plated on 96-well plates (Corning; 3904) at 30,000 cells/well and allowed to grow in complete medium overnight. The cells were then incubated with covalent ligands (50  $\mu$ M or at indicated concentrations), rapamycin (100 nM), Torin 1 (250 nM) or DMSO solvent control in complete medium (100  $\mu$ L) for 24 h. After that, the medium was aspirated and the cells were fixed with 4% paraformaldehyde in PBS (100  $\mu$ L) for 10 min, washed with PBS (100  $\mu$ L) and assayed in PBS (100  $\mu$ L) by SpectraMax i3 (Molecular Devices). GFP fluorescence was measured with excitation and emission at 488 $\pm$ 9 nm and 514 $\pm$ 15 nm respectively, while RFP fluorescence was measured with excitation and emission at 584 $\pm$ 9 nm and 612 $\pm$ 15 nm respectively.

For HEK293A cells stably expressing GFP-LC3-RFP-LC3 G, before they were seeded, 96-well plates were coated with fibronectin in PBS (5  $\mu$ g/mL, 75  $\mu$ L/well) for 1 h at 37 °C. The solution was then aspirated, and cells were plated at 30,000 cells/well, allowed to grow in complete medium overnight, treated and assayed with the same protocol as described above for MEF cells.

For checking cell viability, solutions were aspirated after treatment with the compounds, and the cells were fixed and stained by Hoechst 33342 (13.3  $\mu$ g/mL) in formalin (100  $\mu$ L) for 15 min. After that, cells were washed with PBS (100  $\mu$ L) and assayed in PBS (100  $\mu$ L) by SpectraMax i3 with excitation and emission at 350 $\pm$ 9 nm and 461 $\pm$ 15 nm respectively.

## Transmission electron microscopy

HEK293A cells grown on tissue culture plates were fixed in 2.5% glutaraldehyde 0.1 M sodium cacodylate buffer, pH 7.4 (EMS, Hatfield, PA, USA) for 30 min at room temperature and then gently scraped using a rubber policeman. Cell pellets were stabilized in 1% low melting point agarose, then cut into 1mm cubes. Samples were rinsed (3x; 10 min, room temperature) in 0.1 M sodium cacodylate buffer, pH 7.2, and immersed in 1 % osmium tetroxide with 1.6 % potassium ferricyanide in 0.1 M sodium cacodylate buffer for 1 hour. Samples were rinsed (3x; 10 min, room temperature) in buffer and then in distilled water (3x; 10 min, room temperature). Sample were immersed in 0.5 % aqueous uranyl acetate *en bloc* stain for 1 hour, protected from light and then rinsed in water (3x; 10 min, room temperature). Samples were then subjected to an ascending acetone gradient (10 min; 35 %, 50 %, 70 %, 80 %, 90 %) followed by pure acetone (2x; 10 min, room temperature). Samples were progressively infiltrated while rocking with Epon resin (EMS, Hatfield, PA, USA) and polymerized at 60 °C for 24–48 hours. Thin sections (70 nm) were cut using a Reichert Ultracut E (Leica, Wetzlar, Germany). Sections were then collected onto formvar-coated 200 mesh copper grids. The grids were post-stained with 2 % uranyl acetate followed by Reynold's lead citrate, for 5 min each. The sections were imaged using a Tecnai 12 120kV TEM (FEI, Hillsboro, OR, USA) and data recorded using an UltraScan 1000 with Digital Micrograph 3 software (Gatan Inc., Pleasanton, CA, USA).

## IsoTOP-ABPP chemoproteomic studies

IsoTOP-ABPP studies were done as previously reported<sup>30,31</sup>. Briefly, cells were lysed by probe sonication in PBS and protein concentrations were assessed by BCA assay<sup>51</sup>. Cells were then treated for 90 min with either DMSO vehicle or EN6 (from 1000X DMSO stock). Proteomes were subsequently labeled with IA-alkyne labeling (100  $\mu$ M) for 1 h at room temperature. CuAAC was used by addition sequentially of tris(2-carboxyethyl)phosphine (1 mM, Sigma), tris[(1-benzyl-1H-1,2,3-triazol-4-yl)methyl]amine (34  $\mu$ M, Sigma), copper (II) sulfate (1 mM, Sigma), and biotin-linker-azide—the linker functionalized with a TEV protease recognition sequence as well as an isotopically light or heavy valine for treatment of control or treated proteome, respectively. After CuAAC, proteomes were precipitated, washed in ice-cold methanol, combined in a 1:1 control/treated ratio and washed again. The protein pellet was then denatured and resolubilized by heating in 1.2% SDS/PBS to 80 °C. Insoluble components were precipitated by centrifugation at 6500 x g and soluble proteome was diluted in 5 ml 0.2% SDS/PBS. Labeled proteins were enriched using avidin-agarose beads (Thermo Pierce) by overnight rotating at 4 °C. Enriched proteins were washed on-bead three times in PBS and water. Samples were then resuspended in 6 M urea/PBS (Sigma) and subjected to TCEP reduction (1 mM, Sigma), iodoacetamide (IA) alkylation (18 mM, Sigma), and then washed and resuspended in 2 M urea and subjected to trypsin digestion overnight with sequencing grade trypsin (Promega). Tryptic peptides were eluted off and beads were subsequently washed three times each in PBS and water, washed in TEV buffer solution (water, TEV buffer, 100  $\mu$ M dithiothreitol) and resuspended in buffer with Ac-TEV protease and incubated overnight. Peptides were diluted in water and acidified with formic acid (1.2 M, Spectrum) and prepared for analysis.

## Mass Spectrometry Analysis

Mass spectrometry analysis was performed as previously described<sup>30,31</sup>. Briefly, peptides were pressure-loaded onto a 250  $\mu\text{m}$  inner diameter fused silica capillary tubing packed with 4 cm of Aqua C18 reverse-phase resin (Phenomenex #04A-4299) which was previously equilibrated. The samples were then attached using a MicroTee PEEK 360  $\mu\text{m}$  fitting (Thermo Fisher Scientific #p-888) to a 13 cm laser pulled column packed with 10 cm Aqua C18 reverse-phase resin and 3 cm of strong-cation exchange resin for isoTOP-ABPP studies. Samples were analyzed using an Q Exactive Plus mass spectrometer (Thermo Fisher Scientific) using a 5-step Multidimensional Protein Identification Technology (MudPIT) program. One full MS (MS1) scan (400–1800  $m/z$ ) was followed by 15 MS2 scans (ITMS) of the  $n$ th most abundant ions. Heated capillary temperature was set to 200  $^{\circ}\text{C}$  and the nanospray voltage was set to 2.75 kV.

Data was searched against the Uniprot mouse database using ProLuCID search methodology in IP2 v.3 (Integrated Proteomics Applications, Inc)<sup>52</sup>. Cysteine residues were searched with a static modification for carboxyamino-methylation (+57.02146) and up to two differential modifications for methionine oxidation and either the light or heavy TEV tags (+464.28596 or +470.29977, respectively). Only fully tryptic peptides were analyzed. ProLuCID data was filtered through DTASelect to achieve a peptide false-positive rate below 5%. Only those probe-modified peptides that were evident across two out of three biologically independent groups were interpreted for their isotopic light to heavy ratios. Those probe-modified peptides that showed ratios  $>2.5$  were further analyzed as potential targets of the covalently-acting small-molecule. For modified peptides with ratios  $>2.5$ , we only interpreted peptides that were found across all three biological replicates, showed  $p$ -values  $<0.03$ , and showed high quality MS1 peak shapes across the biological replicates. Light versus heavy isotopic probe-modified peptide ratios are calculated by taking the mean of the ratios of each replicate paired light compared to heavy precursor abundance for all peptide spectral matches (PSM) associated with a peptide. Ratios that were “infinite” or  $>1000$  due to no corresponding heavy or light signal or those ratios  $<0.001$  were replaced with the median ratio of the remaining ratio values. The paired abundances were also used to calculate a paired sample  $t$ -test  $p$ -value in an effort to estimate constancy within paired abundances and significance in change between treatment and control.  $P$ -values were corrected using the Benjamini/Hochberg method.

## Constructing knockdown lines

We used short-hairpin oligonucleotides to knock down the expression of ATP6V1A in HeLa cells using previously described methods<sup>53</sup>. The pLKO.1 lentiviral vector (TRC, Broad institute) was used to express the shRNA against ATP6V1A (TRCN0000029542). ATP6V1A WT or C277A or C277S resistant to the shRNA was cloned into pLKO.1 shRNA vector under the hPGK promoter. For lentivirus production, lentiviral plasmids and packaging plasmids (pMD2.5G, Addgene #12259 and psPAX2, Addgene #12260) were transfected into HEK293T cells using PEI transfection method. Viral supernatant was collected 48 hours after transfection and filtered with 0.45  $\mu\text{m}$  filter. The viruses were further concentrated using Lenti-X Concentrator (Clontech, 631231) according to the manufacturer’s instructions. Target cells were plated in 6-well or 10 cm plates with 8  $\mu\text{g}/\text{mL}$

polybrene (Millipore, TR-1003-G) and incubated with virus containing media. 24 hours later, the media was changed to fresh media containing 2 µg/mL puromycin (Calbiochem, 540411) and selected for over 3 days. Knockdown and protein expression were confirmed by immunoblotting.

### Gel-Based ABPP

Gel-based ABPP methods were performed as previously described<sup>31,54–56</sup>. Pure human ATP6V1A protein was purchased from Abcam (ab132441). Pure protein (0.1 µg) was pre-treated with DMSO vehicle or covalent ligand for 1 h at 37 °C in 50 µL PBS, and were then treated with tetramethylrhodamine-5-iodoacetamide dihydroiodide (IA-rhodamine; 1 µM final concentration) for 1 h at room temperature. Samples were quenched with 4 x reducing Laemmli SDS sample loading buffer (Alfa Aesar) and heated at 90 °C for 5 min. Samples were then separated by molecular weight on precast 4–20% TGX gels (Bio-Rad Laboratories, Inc.) and scanned by ChemiDoc MP (Bio-Rad Laboratories, Inc). Target labeling was quantified by densitometry with ImageJ.

### Resynthesis and characterization of EN6

The initial autophagy screen shown in Fig. 1A used EN6 from our screening plates. All subsequent uses of EN6 in this study are either from resupplied EN6 or resynthesized EN6. Repurchased EN6 was >97 % purity. See supporting information for experimental details.

### Covalent Ligand Library

Synthesis and characterization data of cysteine non-reactive EN6 analog, CC2–49, can be found in Supporting information. Synthesis and characterization of other covalent ligands screened here have been previously reported and were >95 % purity<sup>28–31,57,58</sup>. Compounds that begin with “EN” were obtained from Enamine LLC and were of at least 90 % purity.

### Antibodies and reagents for biological experiments

Antibodies to phospho-T389-S6K1 (9234), S6K1 (2708), phospho-S65–4E-BP1(9451), phospho-T37/46 4E-BP1 (2855), 4E-BP1 (9644), phospho-T308-Akt (13038), phospho-S473-Akt (4060), Akt (4691), phospho-S757-ULK1 (14202), ULK1 (8054), S6 (9202), phospho-S240/244 S6 (5364), LC3B (3868), p62/SQSTM1 (39749), ATP6V1B2 (14617), and FLAG epitope (2368) were from Cell Signaling Technology; Antibody to ATP6V1A (ab137574) was from Abcam; Antibodies to LAMP2 (sc-18822), GFP (sc-9996) and ATP6V1D (sc-390164) were from Santa Cruz Biotechnology. Goat anti-rabbit IgG superclonal secondary antibody-Alexa Fluor 647 (A27040) and anti-mouse IgG superclonal secondary antibody-Alexa Fluor 488 (A228175) were from Thermo Fisher Scientific. IRDye® 800CW Goat anti-Rabbit IgG (H + L; 926–32211) was from Li-Cor. Recombinant human ATP6V1A protein (ab132441) was from Abcam; Tetramethylrhodamine-5-iodoacetamide dihydroiodide (6222) was from Setareh Biotech.; Normal goat serum (10%; 50062Z), Hoechst 33342 (H3570) and LysoSensor Yellow/Blue DND-160 (L7545) were from Thermo Fisher Scientific. Amino acids, Flag-M2 affinity gel (A2220) and Bafilomycin A1 (B1793) from Sigma-Aldrich. Torin 1 (4247) from Tocris Biosciences. Rapamycin was from Selleckchem. Pierce Protease Inhibitor Tablets (A32965) from Thermo Fisher

Scientific. Amino acid-free RPMI (R9010–01) from US Biologicals. Dulbecco's Modified Eagle's Medium (DMEM; 10–013-CV) and fetal bovine serum (FBS; 35–015-CV) were from Corning. 0.25% Trypsin-EDTA (1×; 25200–056) and GlutaMax (100×; 25030–081) were from Thermo Fisher Scientific. Sequencing grade modified trypsin (V51111) was from Promega.

### **Amino acid starvation and stimulation**

Sub-confluent cells were rinsed and incubated with RPMI without amino acids supplemented with 2% dialyzed FBS for 50 min, as described<sup>20</sup>. Stimulation with amino acids (concentration as in RPMI) was performed for 10 min. Where drug treatment was performed, cells were incubated during the 50 min starvation period and the 10 min stimulation period.

### **Western blotting and immunoprecipitation**

Cells were washed twice with ice-cold phosphate-buffered saline (PBS) and lysed in lysis buffer (1% Triton X-100, 10 mM  $\beta$ -glycerol phosphate, 10 mM sodium pyrophosphate, 4 mM EDTA, 40 mM HEPES at pH 7.4, and 1 tablet of EDTA-free protease inhibitors per 50 ml). Cell lysates were cleared by centrifugation in a microcentrifuge at 17,000 x g for 10 minutes at 4 °C. Cell lysate samples were prepared by addition of 5X sample buffer, heated at 95 °C for 5 minutes, resolved by 10% or 12% SDS-PAGE, and analyzed by immunoblotting. Antibodies were obtained from various commercial sources and dilutions were prepared per recommended manufacturers' procedures.

For FLAG immunoprecipitations, HEK293T cells stably expressing Flag-tagged proteins were lysed as above and 30  $\mu$ L of a well-mixed 50% slurry of anti-FLAG M2 Affinity Gel (Sigma A2220) was added to each lysate (1 mg/ml) and incubated at 4 °C in a shaker for 1 hour. Immunoprecipitates were washed four times, three times with lysis buffer and once with lysis buffer containing 400 mM NaCl. Immunoprecipitated proteins were denatured by addition of 50  $\mu$ L of sample buffer and heating to 95 °C for 5 minutes, resolved by SDS-PAGE, and analyzed by immunoblotting.

### **Imaging LC3B puncta in EN6-treated HEK293A cells by confocal fluorescence microscopy**

HEK293A cells were plated on fibronectin-coated (5  $\mu$ g/mL) 8-well Lab Tek borosilicate chambered coverglass slides (Nunc) at 40,000 cells/well and allowed to grow in complete medium overnight. The cells were then incubated with EN6 (at indicated concentrations), Torin 1 (250 nM) or DMSO control for indicated time intervals. After aspiration of the solution, the cells were washed with PBS (350  $\mu$ L) and fixed with methanol for 15 min at –20 °C. The cells were rinsed three times with PBS (350  $\mu$ L each), and incubated with PBS containing 5% normal goat serum and 0.3% Triton X-100 (300  $\mu$ L) for 1 h. The cells were washed with PBS (350  $\mu$ L) and incubated with anti-LC3B (Cell Signaling Technology #3868; v/v, 1:200) in PBS containing 1% BSA and 0.3% Triton X-100 at 4 °C overnight. After that, the cells were washed three times with PBS (350  $\mu$ L each), and incubated with anti-rabbit superclonal secondary antibody-Alexa Fluor 647 (Thermo Fisher Scientific A27040; v/v = 1:500) in PBS containing 1% BSA and 0.3% Triton X-100 in dark at room temperature for 1 h. The cells were washed three times with PBS (350  $\mu$ L each) and stained

with Hoechst 33342 (5 µg/mL) in PBS in dark at room temperature for 15 min. After washing with PBS three times (350 µL each), the cells were imaged in PBS by Zeiss laser scanning microscope (LSM) 710 with a 20× or 63× oil-immersion objective lens. Hoechst 33342 was excited with a 405 nm diode laser, and emission was collected on a META detector between 410 and 587 nm. Alexa Fluor 647 was excited with a 633 nm HeNe laser, and emission was collected on a META detector between 638 and 755 nm.

Image analysis was performed by use of ImageJ. A threshold of 100–255 (for 8-bit images) was first set for selection of LC3B puncta, and a region of interest (ROI) was created over a single cell. The number of cellular LC3B puncta was then quantified by “Analyze Particles” using size and circularity of 0.1–infinity and 0.0–1.0 respectively. 25 individual cells of each group from triplicate experiments were analyzed, and the statistical analyses were performed with a two-tailed Student’s t-test (MS Excel).

### Imaging TFEB cellular localization

Hela cells stably expressing TFEB-GFP were seeded on glass coverslips coated with fibronectin and incubated for 24hrs. After incubation, cells were treated with either DMSO or EN6 for 4 hours, fixed for 10 min with 4% paraformaldehyde (PFA) and were subsequently mounted on slides using Vectashield. Images were taken using a Nikon Eclipse Ti microscope with Andor Zyla-4.5 sCMOS camera, as mentioned above. 5 different fields were acquired per condition and TFEB localization were assessed.

### Imaging lysosomal recruitment of mTORC1 by immunofluorescence

HEK293T or Hela cells were seeded on fibronectin-coated glass coverslips and allowed to attach overnight. On the following day, cells were subjected to either amino acid starvation and stimulation with or without drug incubation and fixed in 4% paraformaldehyde (PFA) for 15 minutes at room temperature. The coverslips were rinsed twice with PBS and cells were permeabilized with 0.1% (w/v) saponin in PBS for 10 minutes. After rinsing twice with PBS, the slides were incubated with primary antibodies in 5% normal donkey serum (Jackson ImmunoResearch, 017-000-121) for 1 hour at room temperature, rinsed four times with PBS, and fluorophore conjugated secondary antibodies derived from goat or donkey (Life Technologies, diluted 1:400 in 5% normal donkey serum) were incubated for 1 hour at room temperature in the dark. The coverslips were then washed four times with PBS, mounted on glass slides using Vectashield (Vector Laboratories) and imaged on a spinning disk confocal system built upon a Nikon Eclipse Ti microscope with Andor Zyla-4.5 sCMOS camera.

### Imaging lysosomal pH by LysoSensor DND-160

HEK293A cells were plated on fibronectin-coated (5 µg/mL) 12 mm glass based dishes (Nunc) at 1,000,000 cells/well and allowed to grow in complete medium overnight. The cells were then incubated with DMSO control, EN6 (50 µM), bafilomycin A1 (0.2 µM), or a mixture of EN6 and bafilomycin A1 (50 and 0.2 µM respectively) at 37 °C for 4 h. After that, LysoSensor DND-160 (2 µM final concentration) was added to the solution and the cells were stained at 37 °C for 5 min. The solution was then replaced by DPBS and the live cells were imaged by Zeiss LSM 880 with a 40× water-immersion objective lens. The blue

fluorescence of DND-160,  $F_{\text{blue}}$ , was excited with a two-photon laser at 730 nm and emission was collected on a META detector between 400 and 490 nm. The yellow fluorescence of DND-160,  $F_{\text{yellow}}$ , was excited with a two-photon laser at 730 nm and emission was collected on a META detector between 514 and 649 nm.

For converting  $F_{\text{yellow}} / F_{\text{blue}}$  to pHs, a pH calibration curve was constructed from HEK293A cells stained with DND-160 (2  $\mu\text{M}$ ) in DPBS at 37 °C for 5 min, washed by PBS, incubated with different pH buffer solutions (pH 3.5, 4.5, 5.0 and 5.5) in the presence of Valinomycin (10  $\mu\text{M}$ ) and Nigericin (10  $\mu\text{M}$ ) at 37 °C for 5 min, and imaged by LSM 880 with two-photon excitation at 730 nm and emissions collected at 400–490 nm and 514–649 nm for  $F_{\text{blue}}$  and  $F_{\text{yellow}}$  respectively.

The ratiometric images,  $F_{\text{yellow}} / F_{\text{blue}}$ , were generated by Ratio Plus plugin of ImageJ. For quantification, a threshold value was set as background and the average intensity of the whole image was measured by ImageJ. All experiments were performed in triplicate, and statistical analyses were performed with a two-tailed Student's t-test (MS excel).

### **In vitro v-ATPase assays**

The experiment was performed as previously described<sup>18</sup>. In brief, two 15cm confluent HEK293T cells were incubated overnight with 30  $\mu\text{g}/\text{ml}$  70 kDa Dextran conjugated to Oregon Green 514 (Dx-OG514, Invitrogen). The next day, cells were washed and chased for 2 hours in serum free DMEM to allow lysosomal accumulation of Dx-OG514. 15 minutes prior to lysis, 1  $\mu\text{M}$  FCCP was added to dissipate the lysosomal pH gradient. Cells were then harvested and mechanically broken using a 23 G needle in fractional buffer: 140 mM KCl, 1 mM EGTA, 20 mM HEPES, 50 mM Sucrose (pH 7.4), supplemented with 5 mM Glucose, protease inhibitor and 1  $\mu\text{M}$  FCCP. Lysed cells were spun down at 1700 rpm for 10 min at 4°C and the supernatant was collected. The resulting post-nuclear supernatant (PNS) was spun down at max speed at 4°C, yielding a pellet containing the organellar fraction. Each fraction was resuspended in 180  $\mu\text{l}$  of fractionation buffer devoid of FCCP and transferred to a 96-multiwell (black). Baseline fluorescence was collected at 530 nm upon 490 nm excitation in SpectraMax i3 at 30sec intervals for 5 min. Various compounds were added to each well followed by 5 mM ATP and  $\text{MgCl}_2$ , and fluorescence reading was resumed for further 45 min. The fluorescence emission of Dx-OG514 decayed exponentially over time due to the lysosomal reacidification of the v-ATPase.

### **RNA extraction and quantitative RT-PCR (qRT-PCR)**

Total RNAs were extracted using Aurum<sup>TM</sup> Total RNA Mini Kit (Bio-rad) and reverse transcription was performed from 1  $\mu\text{g}$  total RNAs using iScript<sup>TM</sup> Reverse Transcription for RT-qPCR (Bio-rad) according to manufacturer's instruction. All real-time qPCR (qRT-PCR) analyses were performed using StepOnePlus machine (Applied Biosystems) with SsoAdvanced<sup>TM</sup> Universal SYBR Green supermix (Bio-rad).

The quantity of mRNA was calculated using the  $C_t$  method and normalized to  $\beta$ -actin. All reactions were performed as triplicates.



### Assessing TDP-43 aggregates

U2OS cells stably expressing an IPTG-inducible GFP-TDP-43 (Innoprot) were plated on fibronectin-coated (5 µg/mL) 8-well Lab Tek borosilicate chambered coverglass slides (Nunc) at 30,000 cells/well and allowed to grow in complete medium overnight. For co-incubation experiments, the cells were incubated with DMSO control, isopropylthio-β-galactoside (IPTG; 50 µM), a mixture of EN6 (25 µM) and IPTG (50 µM), or a mixture of EN6 (25 µM), IPTG (50 µM) and bafilomycin A1 (0.2 µM) at 37 °C for 7 h. The cells were washed with PBS (350 µL) and fixed with 4% paraformaldehyde (PFA) for 15 minutes at room temperature. After fixation, the cells were washed three times with PBS (350 µL each) and stained with Hoechst 33342 (0.5 µg/mL) in PBS in dark at room temperature for 15 min. After washing with PBS three times (350 µL each), the cells were imaged in PBS by Zeiss laser scanning microscope (LSM) 710 with a 20× or 63× oil-immersion objective lens. Hoechst 33342 was excited with a 405 nm diode laser, and emission was collected on a META detector between 410 and 483 nm. GFP was excited with a 488 nm Ar laser, and emission was collected on a META detector between 493 and 598 nm.

For pre-stimulation experiments, U2OS cells stably expressing an IPTG-inducible GFP-TDP-43 were pre-treated with IPTG (1 mM) at 37 °C for 4 h to express GFP-TDP-43 aggregates. Then, the cells were treated with DMSO control or EN6 (25 µM) at 37 °C for 4 h. The treated cells were washed, fixed and imaged as described above for visualizing TDP-43 aggregates by GFP fluorescence. For visualizing TDP-43 aggregates by anti-GFP immunofluorescence, cells after treatment with DMSO and EN6 were washed with PBS (350 µL) and fixed with 4% paraformaldehyde (PFA) for 15 minutes at room temperature. After fixation, the cells were washed three times with PBS (350 µL each), incubated with PBS containing 1% BSA and 0.3% Triton X-100 at room temperature for 1 h, and incubated with mouse anti-GFP (sc-9996; 1:100 dilution) in PBS containing 1% BSA and 0.3% Triton X-100 at 4 °C overnight. Then, the cells were washed with PBS containing 1% BSA and 0.3% Triton X-100 three times, and incubated with anti-mouse IgG superclonal secondary antibody-Alexa Fluor 488 (A228175; 1:500 dilution) in PBS containing 1% BSA and 0.3% Triton X-100 at room temperature for 1 h. After washing with PBS containing 1% BSA and 0.3% Triton X-100 three times, the cells were stained with Hoechst 33342 (0.5 µg/mL) in PBS in dark at room temperature for 15 min, washing with PBS three times and imaged in PBS by Zeiss laser scanning microscope (LSM) 710 with a 20× or 63× oil-immersion objective lens. Hoechst 33342 was excited with a 405 nm diode laser, and emission was collected on a META detector between 410 and 483 nm. Anti-GFP immunofluorescence was collected on a META detector between 493 and 630 nm with excitation at 488 nm by Ar laser.

Image analysis was performed by use of ImageJ. A threshold was first set for selection of GFP-TDP-43 aggregate, and a region of interest (ROI) was created over a single cell. The number of cellular aggregates was then quantified by “Analyze Particles” using size and circularity of 0.3–infinity and 0.0–1.0 respectively. 26 individual cells of each group from triplicate experiments were analyzed, and the statistical analyses were performed with a two-tailed Student’s t-test (MS Excel).

## Assessing mTORC1 inhibition *in vivo* and pharmacokinetics of EN6 in mice

6-week-old male C57BL/6 mice (Jackson Laboratory) were injected intraperitoneally with solvent control, EN6 (50 mg/kg) or rapamycin (10 mg/kg) in saline/ethanol/PEG-40 (v/v/v = 18:1:1). After 4 h, mice were euthanized, and tissues were harvested and lysed in lysis buffer (1% Triton X-100, 10 mM  $\beta$ -glycerol phosphate, 10 mM sodium pyrophosphate, 4 mM EDTA, 40 mM HEPES at pH 7.4, and 1 tablet of EDTA-free protease inhibitors per 50 ml) at 4 °C for 30 min. The lysates were cleared by centrifugation in a microcentrifuge at 21,130 g for 10 minutes at 4 °C and protein concentration of supernatant was determined by BCA assay (Thermo Fisher Scientific). The lysates were then diluted to 1.5 mg/mL, mixed with 4× sample buffer, heated at 95 °C for 5 minutes, resolved by precast 4–20% TGX gels, and analyzed by immunoblotting. Antibodies were obtained from various commercial sources and dilutions were prepared per recommended manufacturers' procedures.

For pharmacokinetics studies, mice were injected intraperitoneally with solvent control or EN6 at indicated doses. At indicated time intervals, mice were euthanized, and tissues were harvested. The tissues were then weighed and homogenized, and EN6 was extracted from chloroform:methanol:PBS solution mixture (2:1:1, v/v/v; 4 mL total) with dodecylglycerol (10 nmol) as internal standard. The organic layer was collected, evaporated under stream of N<sub>2</sub>, re-dispersed in chloroform and analyzed by multiple-reaction monitoring (MRM)-based targeted LC-MS/MS on an Agilent 6430 QQQ using a Luna reverse phase C5 column (50 mm × 4.6 mm with 5 mm diameter particles, Phenomenex). Mobile phases: Buffer A, 95:5 water / methanol; Buffer B: 60:35:5 2-propanol / methanol / water, both with 0.1 % formic acid and 50 mM ammonium formate additives. Flow rate began at 0.2 mL/min for 2 min, followed by a gradient starting at 0 % B and increasing linearly to 100 % B over the course of 23 min with a flow rate of 0.4 mL/min, followed by an isocratic gradient of 100 % B for 5 min with a flow rate increasing linearly from 0.04 mL/min to 0.4 mL/min. MS analysis was performed using electrospray ionization (ESI) with a drying gas temperature of 350 °C, drying gas flow rate of 10 L/min, nebulizer pressure 35 psi, capillary voltage 3.0 kV, and fragmentor voltage 100 V. Parent/daughter ion MRM transitions used to determine EN6 levels were 369.34/163.2 and 369.34/189 with fragmentor voltage of 10 and 20, and 30 and 40, respectively. Peak area of EN6 to that of dodecylglycerol was calibrated to amount of EN6 per gram of tissues by LC-MS/MS analysis of a set of solution mixtures containing dodecylglycerol (10 nmol) and known concentrations of EN6 (0.01, 0.1, 1, 10 and 30 nmol). Data was analyzed using Agilent Qualitative Analysis software by calculating area under the curve.

All animal experiments were conducted in accordance with the guidelines of the Institutional Animal Care and Use Committees of the University of California, Berkeley.

## Supplementary Material

Refer to Web version on PubMed Central for supplementary material.

## Acknowledgement

We thank the members of the Nomura Research Group and the Zoncu lab and Novartis Institutes for BioMedical Research for critical reading of the manuscript. This work was supported by Novartis Institutes for BioMedical

Research and the Novartis-Berkeley Center for Proteomics and Chemistry Technologies (NB-CPACT) for CYSC, CAB, BF, CCW, and DKN, National Institutes of Health (NIEHS R01ES028096 for DKN and CYSC, NCI F31CA225173 for CCW, and NCI DP2CA195761 for RZ and NIGMS R01GM112948 for JAO), the Shurl & Kay Curci Foundation Faculty Scholars grant (RZ) and the National Research Foundation (NRF) funded by the South Korean government for HRS (2017R1C1B2007409). Confocal imaging experiments were conducted at the CRL Molecular Imaging Center, supported by the Helen Wills Neuroscience Institute and Gordon and Betty Moore Foundation (UC Berkeley). We would like to thank Holly Aaron and Feather Ives for their microscopy training and assistance. We also thank Reena Zalpuri at the University of California Berkeley Electron Microscope Laboratory for advice and assistance in electron microscopy sample preparation and data collection.

#### Competing Financial Interests Statement

This study was funded by the Novartis Institutes for BioMedical Research and the Novartis-Berkeley Center for Proteomics and Chemistry Technologies. DKN is the director of the Novartis-Berkeley Center for Proteomics and Chemistry Technologies. DKN is a co-founder, share-holder, and adviser for Artris Therapeutics and Frontier Medicines. RZ is a co-founder, share-holder, and adviser for Frontier Medicines.

## References

1. Khaminets A, Behl C & Dikic I Ubiquitin-Dependent And Independent Signals In Selective Autophagy. *Trends Cell Biol.* 26, 6–16 (2016). [PubMed: 26437584]
2. Rubinsztein DC, Codogno P & Levine B Autophagy modulation as a potential therapeutic target for diverse diseases. *Nat. Rev. Drug Discov* 11, 709–730 (2012). [PubMed: 22935804]
3. Galluzzi L, Bravo-San Pedro JM, Levine B, Green DR & Kroemer G Pharmacological modulation of autophagy: therapeutic potential and persisting obstacles. *Nat. Rev. Drug Discov* 16, 487–511 (2017). [PubMed: 28529316]
4. Dikic I & Elazar Z Mechanism and medical implications of mammalian autophagy. *Nat. Rev. Mol. Cell Biol* 19, 349–364 (2018). [PubMed: 29618831]
5. Perera RM & Zoncu R The Lysosome as a Regulatory Hub. *Annu. Rev. Cell Dev. Biol* 32, 223–253 (2016). [PubMed: 27501449]
6. Saxton RA & Sabatini DM mTOR Signaling in Growth, Metabolism, and Disease. *Cell* 169, 361–371 (2017).
7. Settembre C et al. A lysosome-to-nucleus signalling mechanism senses and regulates the lysosome via mTOR and TFEB. *EMBO J.* 31, 1095–1108 (2012). [PubMed: 22343943]
8. Menzies FM, Fleming A & Rubinsztein DC Compromised autophagy and neurodegenerative diseases. *Nat. Rev. Neurosci* 16, 345–357 (2015). [PubMed: 25991442]
9. Barmada SJ et al. Autophagy induction enhances TDP43 turnover and survival in neuronal ALS models. *Nat. Chem. Biol* 10, 677–685 (2014). [PubMed: 24974230]
10. Tsvetkov AS et al. A small-molecule scaffold induces autophagy in primary neurons and protects against toxicity in a Huntington disease model. *Proc. Natl. Acad. Sci. U. S. A* 107, 16982–16987 (2010). [PubMed: 20833817]
11. Fu Y et al. A toxic mutant huntingtin species is resistant to selective autophagy. *Nat. Chem. Biol* 13, 1152–1154 (2017). [PubMed: 28869595]
12. Fox JH et al. The mTOR kinase inhibitor Everolimus decreases S6 kinase phosphorylation but fails to reduce mutant huntingtin levels in brain and is not neuroprotective in the R6/2 mouse model of Huntington’s disease. *Mol. Neurodegener* 5, 26 (2010). [PubMed: 20569486]
13. Duarte-Silva S et al. Combined therapy with m-TOR-dependent and -independent autophagy inducers causes neurotoxicity in a mouse model of Machado-Joseph disease. *Neuroscience* 313, 162–173 (2016). [PubMed: 26601773]
14. Ghosh A & Greenberg ME Distinct roles for bFGF and NT-3 in the regulation of cortical neurogenesis. *Neuron* 15, 89–103 (1995). [PubMed: 7619533]
15. Kuruvilla R, Ye H & Ginty DD Spatially and functionally distinct roles of the PI3-K effector pathway during NGF signaling in sympathetic neurons. *Neuron* 27, 499–512 (2000). [PubMed: 11055433]
16. Brunet A et al. Akt promotes cell survival by phosphorylating and inhibiting a Forkhead transcription factor. *Cell* 96, 857–868 (1999). [PubMed: 10102273]

17. Sancak Y et al. Ragulator-Rag complex targets mTORC1 to the lysosomal surface and is necessary for its activation by amino acids. *Cell* 141, 290–303 (2010). [PubMed: 20381137]
18. Zoncu R et al. mTORC1 senses lysosomal amino acids through an inside-out mechanism that requires the vacuolar H(+)-ATPase. *Science* 334, 678–683 (2011). [PubMed: 22053050]
19. Castellano BM et al. Lysosomal cholesterol activates mTORC1 via an SLC38A9-Niemann-Pick C1 signaling complex. *Science* 355, 1306–1311 (2017). [PubMed: 28336668]
20. Sancak Y et al. The Rag GTPases bind raptor and mediate amino acid signaling to mTORC1. *Science* 320, 1496–1501 (2008). [PubMed: 18497260]
21. Kim E, Goraksha-Hicks P, Li L, Neufeld TP & Guan K-L Regulation of TORC1 by Rag GTPases in nutrient response. *Nat. Cell Biol* 10, 935–945 (2008). [PubMed: 18604198]
22. Forgac M Vacuolar ATPases: rotary proton pumps in physiology and pathophysiology. *Nat. Rev. Mol. Cell Biol* 8, 917–929 (2007). [PubMed: 17912264]
23. Zhao J, Benlekhir S & Rubinstein JL Electron cryomicroscopy observation of rotational states in a eukaryotic V-ATPase. *Nature* 521, 241–245 (2015). [PubMed: 25971514]
24. Jewell JL et al. Metabolism. Differential regulation of mTORC1 by leucine and glutamine. *Science* 347, 194–198 (2015). [PubMed: 25567907]
25. Dechant R, Saad S, Ibáñez AJ & Peter M Cytosolic pH regulates cell growth through distinct GTPases, Arf1 and Gtr1, to promote Ras/PKA and TORC1 activity. *Mol. Cell* 55, 409–421 (2014). [PubMed: 25002144]
26. Bar-Peled L, Schweitzer LD, Zoncu R & Sabatini DM Ragulator is a GEF for the rag GTPases that signal amino acid levels to mTORC1. *Cell* 150, 1196–1208 (2012). [PubMed: 22980980]
27. Kaizuka T et al. An Autophagic Flux Probe that Releases an Internal Control. *Mol. Cell* 64, 835–849 (2016). [PubMed: 27818143]
28. Spradlin JN et al. Harnessing the Anti-Cancer Natural Product Nimbolide for Targeted Protein Degradation. *bioRxiv* 436998 (2018). doi:10.1101/436998
29. Anderson KE, To M, Olzmann JA & Nomura DK Chemoproteomics-Enabled Covalent Ligand Screening Reveals a Thioredoxin-Caspase 3 Interaction Disruptor That Impairs Breast Cancer Pathogenicity. *ACS Chem. Biol* 12, 2522–2528 (2017). [PubMed: 28892616]
30. Grossman EA et al. Covalent Ligand Discovery against Druggable Hotspots Targeted by Anti-cancer Natural Products. *Cell Chem. Biol* 24, 1368–1376.e4 (2017). [PubMed: 28919038]
31. Bateman LA et al. Chemoproteomics-enabled covalent ligand screen reveals a cysteine hotspot in reticulin 4 that impairs ER morphology and cancer pathogenicity. *Chem. Commun. Camb. Engl* 53, 7234–7237 (2017).
32. Weerapana E et al. Quantitative reactivity profiling predicts functional cysteines in proteomes. *Nature* 468, 790–795 (2010). [PubMed: 21085121]
33. Backus KM et al. Proteome-wide covalent ligand discovery in native biological systems. *Nature* 534, 570–574 (2016). [PubMed: 27309814]
34. Chen Y-C et al. Covalent Modulators of the Vacuolar ATPase. *J. Am. Chem. Soc* 139, 639–642 (2017). [PubMed: 28010062]
35. Steinberg BE et al. A cation counterflux supports lysosomal acidification. *J. Cell Biol* 189, 1171–1186 (2010). [PubMed: 20566682]
36. Bar-Peled L et al. A Tumor suppressor complex with GAP activity for the Rag GTPases that signal amino acid sufficiency to mTORC1. *Science* 340, 1100–1106 (2013). [PubMed: 23723238]
37. Rocznik-Ferguson A et al. The transcription factor TFEB links mTORC1 signaling to transcriptional control of lysosome homeostasis. *Sci. Signal* 5, ra42 (2012). [PubMed: 22692423]
38. Martina JA, Chen Y, Gucek M & Puertollano R MTORC1 functions as a transcriptional regulator of autophagy by preventing nuclear transport of TFEB. *Autophagy* 8, 903–914 (2012). [PubMed: 22576015]
39. Sreedharan J et al. TDP-43 Mutations in Familial and Sporadic Amyotrophic Lateral Sclerosis. *Science* 319, 1668–1672 (2008). [PubMed: 18309045]
40. Inhibition of mTORC1 signaling in aged rats counteracts the decline in muscle mass and reverses multiple parameters of muscle signaling associated with sarcopenia | *bioRxiv*. Available at: <https://www.biorxiv.org/content/10.1101/591891v1>. (Accessed: 3rd April 2019)

41. Ramos FJ et al. Rapamycin Reverses Elevated mTORC1 Signaling in Lamin A/C–Deficient Mice, Rescues Cardiac and Skeletal Muscle Function, and Extends Survival. *Sci. Transl. Med* 4, 144ra103–144ra103 (2012).
42. Masiero E et al. Autophagy Is Required to Maintain Muscle Mass. *Cell Metab.* 10, 507–515 (2009). [PubMed: 19945408]
43. Yano T et al. Clinical impact of myocardial mTORC1 activation in nonischemic dilated cardiomyopathy. *J. Mol. Cell. Cardiol* 91, 6–9 (2016). [PubMed: 26739211]
44. Thoreen CC et al. An ATP-competitive mammalian target of rapamycin inhibitor reveals rapamycin-resistant functions of mTORC1. *J. Biol. Chem* 284, 8023–8032 (2009). [PubMed: 19150980]
45. Rodrik-Outmezguine VS et al. Overcoming mTOR resistance mutations with a new-generation mTOR inhibitor. *Nature* 534, 272–276 (2016). [PubMed: 27279227]
46. García-Martínez JM et al. Ku-0063794 is a specific inhibitor of the mammalian target of rapamycin (mTOR). *Biochem. J* 421, 29–42 (2009). [PubMed: 19402821]
47. Sarbassov DD et al. Prolonged rapamycin treatment inhibits mTORC2 assembly and Akt/PKB. *Mol. Cell* 22, 159–168 (2006). [PubMed: 16603397]
48. Lamming DW et al. Rapamycin-induced insulin resistance is mediated by mTORC2 loss and uncoupled from longevity. *Science* 335, 1638–1643 (2012). [PubMed: 22461615]
49. Arai S et al. Rotation mechanism of *Enterococcus hirae* V1-ATPase based on asymmetric crystal structures. *Nature* 493, 703–707 (2013). [PubMed: 23334411]
50. Mazhab-Jafari MT et al. Atomic model for the membrane-embedded VO motor of a eukaryotic V-ATPase. *Nature* 539, 118–122 (2016). [PubMed: 27776355]
51. Smith PK et al. Measurement of protein using bicinchoninic acid. *Anal. Biochem* 150, 76–85 (1985). [PubMed: 3843705]
52. Xu T et al. ProLuCID: An improved SEQUEST-like algorithm with enhanced sensitivity and specificity. *J. Proteomics* 129, 16–24 (2015). [PubMed: 26171723]
53. Benjamin DI et al. Ether lipid generating enzyme AGPS alters the balance of structural and signaling lipids to fuel cancer pathogenicity. *Proc. Natl. Acad. Sci. U. S. A* 110, 14912–14917 (2013). [PubMed: 23980144]
54. Counihan JL, Wiggenhorn AL, Anderson KE & Nomura DK Chemoproteomics-Enabled Covalent Ligand Screening Reveals ALDH3A1 as a Lung Cancer Therapy Target. *ACS Chem. Biol* (2018). doi:10.1021/acscchembio.8b00381
55. Louie SM et al. GSTP1 Is a Driver of Triple-Negative Breast Cancer Cell Metabolism and Pathogenicity. *Cell Chem. Biol* 23, 567–578 (2016). [PubMed: 27185638]
56. Medina-Cleghorn D et al. Mapping Proteome-Wide Targets of Environmental Chemicals Using Reactivity-Based Chemoproteomic Platforms. *Chem. Biol* 22, 1394–1405 (2015). [PubMed: 26496688]
57. Roberts AM et al. Chemoproteomic Screening of Covalent Ligands Reveals UBA5 As a Novel Pancreatic Cancer Target. *ACS Chem. Biol* 12, 899–904 (2017). [PubMed: 28186401]
58. Ward CC et al. Covalent Ligand Screening Uncovers a RNF4 E3 Ligase Recruiter for Targeted Protein Degradation Applications. *bioRxiv* 439125 (2018). doi:10.1101/439125

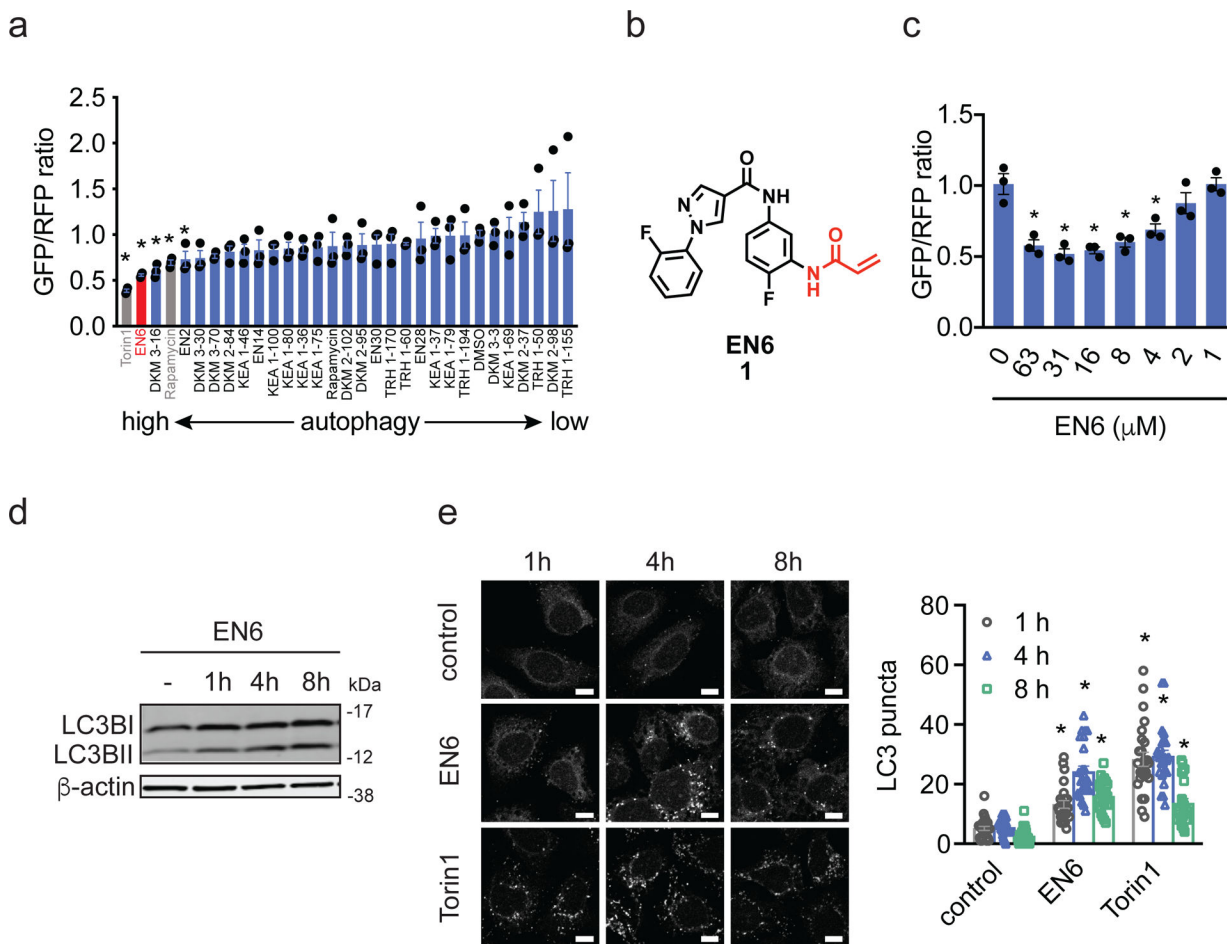


**Figure 1. Covalent ligand screen for autophagy activators.**

(a) Testing autophagy activator hits from covalent ligand screen in MEF cells. HEK293A cells expressing a fluorescent probe GFP-LC3-RFP-LC3 G to measure autophagic flux, were treated with vehicle DMSO or a covalent ligand (50 μM) for 24 h and GFP/RFP ratios were analyzed. Compounds that showed significantly ( $p < 0.05$  compared to vehicle-treated controls) lower GFP/RFP ratios in MEF cells were screened in HEK293A cells expressing the same fluorescent autophagic flux probe. Shown in gray are mTORC1 inhibitors Torin1 and rapamycin and shown in red is the EN6 hit. (b) Structure of cysteine-reactive covalent ligand hit EN6 that shows autophagy activation in both MEF and HEK293A cells. (c) Dose-response of EN6 in HEK293A cells expressing the fluorescent autophagic flux probe. (d) LC3B levels in HEK293A cells treated with EN6 (50 μM). Shown is a representative gel from  $n=3$  biologically independent samples/group. Original gel images can be found in Supplementary Fig. 7a. (e) LC3B puncta in HEK293A cells treated with vehicle DMSO, EN6 (50 μM), or Torin1 (0.25 μM). Scale bar shown in (e) denotes 10 μm. Data shown in (a, c) are average  $\pm$  sem,  $n=3$  biologically independent samples/group, and data shown in (e) are average  $\pm$  sem,  $n=25$  individual cells from 3 biologically independent samples/group. Statistical significance was calculated with unpaired two-tailed Student's *t*-tests. Significance is expressed as \* $p=0.0022$ , 0.0069, 0.00283, 0.027, 0.0495 for Torin1, EN6, DKM 3–16, rapamycin, and EN2, respectively, compared to vehicle-treated controls in (a);

\*p=0.0064, 0.0037, 0.0037, 0.0069, and 0.018 for 63, 31, 16, 8, 4  $\mu$ M EN6, respectively, compared to vehicle-treated controls in **(b)**; \*p= $1.1 \times 10^{-6}$ ,  $4.2 \times 10^{-13}$ ,  $6.4 \times 10^{-16}$  for 1, 4, 8 h EN6 treatment and \*p= $2.1 \times 10^{-12}$ ,  $8.1 \times 10^{-16}$ ,  $1.5 \times 10^{-8}$  for 1, 4, 8 h Torin1 treatment, respectively, compared to vehicle-treated control groups.

Author Manuscript

Author Manuscript

Author Manuscript

Author Manuscript

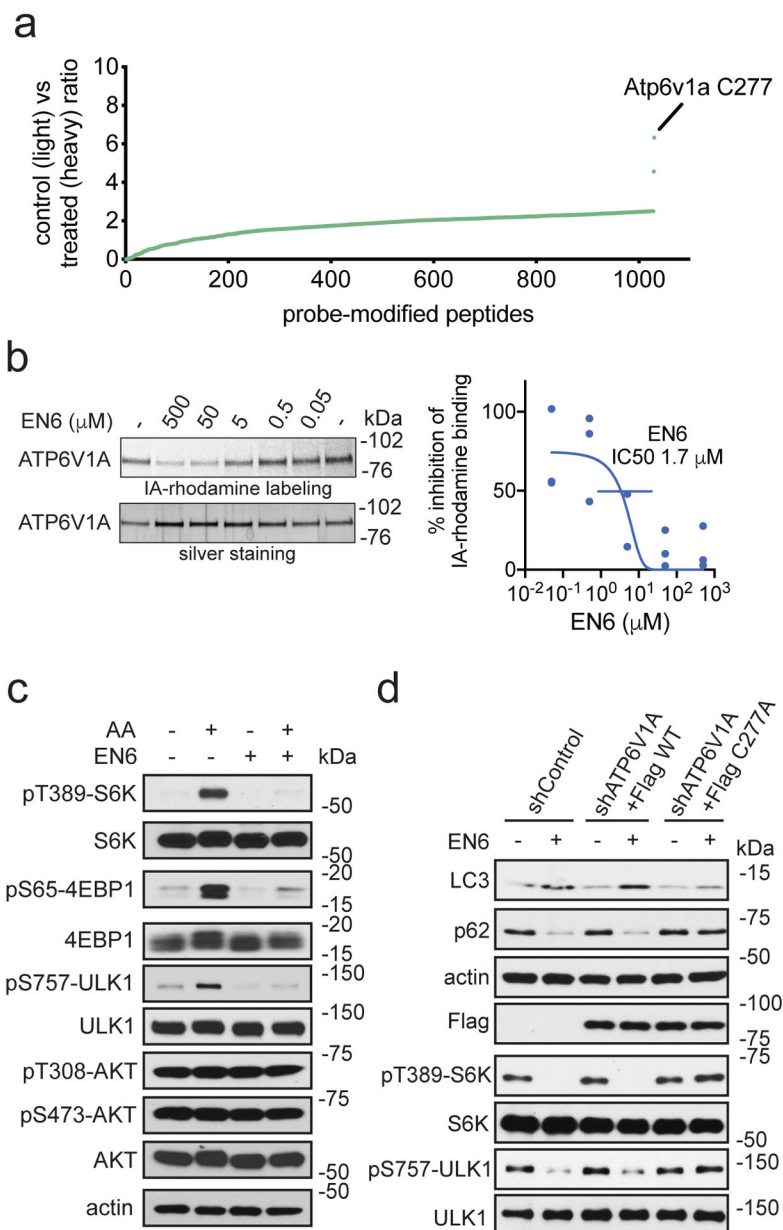


**Figure 2. Target identification and validation of EN6.**

(a) isoTOP-ABPP analysis of EN6 in MEF cells *in situ*. MEF cells were pre-treated with DMSO or EN6 (50  $\mu\text{M}$ , 4 h *in situ*) prior to labeling of proteomes *in vitro* with IA-alkyne (100  $\mu\text{M}$ , 1 h), followed by appendage of isotopically light (for DMSO-treated) or heavy (for EN6-treated) TEV protease cleavable biotin-azide tags by copper-catalyzed azide-alkyne cycloaddition (CuAAC), followed by the isoTOP-ABPP procedure. Shown are average light/heavy ratios for n=3 biologically independent samples/group. More detailed data and individual replicate ratios can be found in Supplementary Dataset 2. (b) Gel-based ABPP analysis of EN6 interactions with recombinant ATP6V1A. Vehicle DMSO or EN6 were pre-incubated with recombinant human ATP6V1A (1 h) followed by labeling with a rhodamine-functionalized iodoacetamide probe (IA-rhodamine) (1  $\mu\text{M}$ , 1 h) after which probe-labeled



proteins were read-out by SDS/PAGE and in-gel fluorescence. Data were quantified by densitometry using Image J. Original gel images can be found in Supplementary Fig. 8a. **(c)** mTORC1 signaling with EN6 treatment in HEK293A cells. HEK293A cells, starved or stimulated with amino acids, were treated with vehicle DMSO or EN6 (25  $\mu$ M) for 1 h and mTORC1 signaling was assessed by Western blotting. Original gel images are in Supplementary Fig. 7b. **(d)** Autophagy markers (LC3 and p62) and mTORC1 signaling in Hela cells treated with EN6. Endogenous ATP6V1A was knocked down with shRNA and replaced with a Flag-tagged wild-type or C277A mutant ATP6V1A and these cells were treated with EN6 (25  $\mu$ M) for 4 h. Original gel images can be found in Supplementary Fig. 8b. Validation of ATP6V1A knockdown can be found in Supplementary Fig. 2e. Data shown in **(b)** are average  $\pm$  sem from n=3 biologically independent samples/group. Gels shown in **(b, c, d)** are representative gels from n=3 biologically independent samples/group.

Author Manuscript

Author Manuscript

Author Manuscript

Author Manuscript

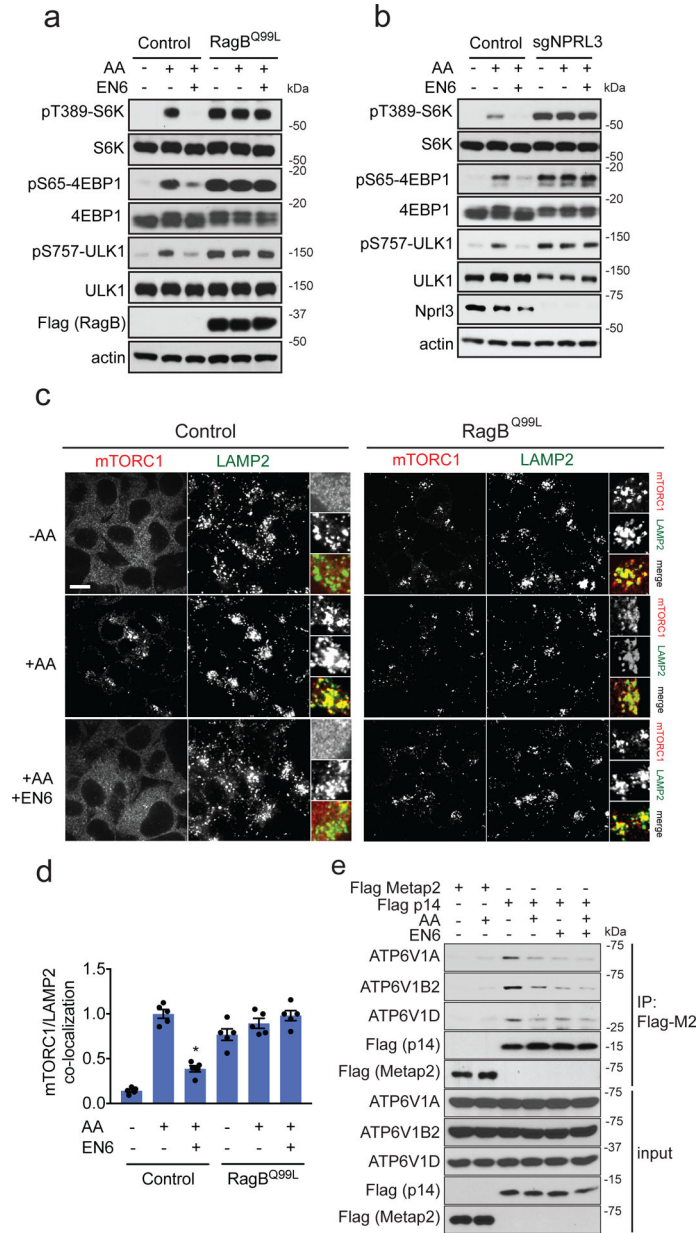


**Figure 3. EN6 inhibits mTORC1 recruitment to the lysosome.** **(a)** mTORC1 signaling in HEK293T cells expressing either control empty vector or Flag-tagged RagB<sup>Q99L</sup> constitutively active mutant protein. Cells were starved of amino acids or starved and stimulated with amino acids, in the presence of DMSO vehicle or EN6 for (25 μM) for 4 h. Original gel images are in Supplementary Fig. 9a. **(b)** mTORC1 signaling in NPRL3 control and knockout HEK293T cells, starved or starved and stimulated with amino acids, in the presence of DMSO vehicle or EN6 for (25 μM) for 4 h. Original gel images are in Supplementary Fig. 9b. **(c)** mTORC1 localization in HEK293T cells expressing either control empty vector or RagB<sup>Q99L</sup> constitutively active mutant protein with vehicle DMSO or EN6 (25 μM) for 1 h under amino acid starvation or stimulation. Shown are representative microscopy images of mTORC1 or the lysosomal marker LAMP2. Scale bar in (c) denotes

10  $\mu\text{m}$ . **(d)** Quantification of mTORC1 lysosomal localization in **(c)**. Data are shown as average  $\pm$  sem from  $n=5$  biologically independent samples/group. Statistical significance was calculated with unpaired two-tailed Student's t-tests. Significance is expressed as  $*p=7.9\times 10^{-6}$  in **(d)** compared to amino acid-stimulated vehicle-treated control. **(e)** Co-immunoprecipitation experiments between stably expressed, FLAG-tagged Ragulator subunit p14 and endogenous v-ATPase components in HEK293T cells, in the absence or presence of amino acids treated with vehicle DMSO or EN6 (25  $\mu\text{M}$ ) for 1 h. Original gel images are in Supplementary Fig. 10. Blots shown are representative gels from  $n=2$  in **(a, b)** and  $n=3$  in **(e)** biologically independent samples/group.

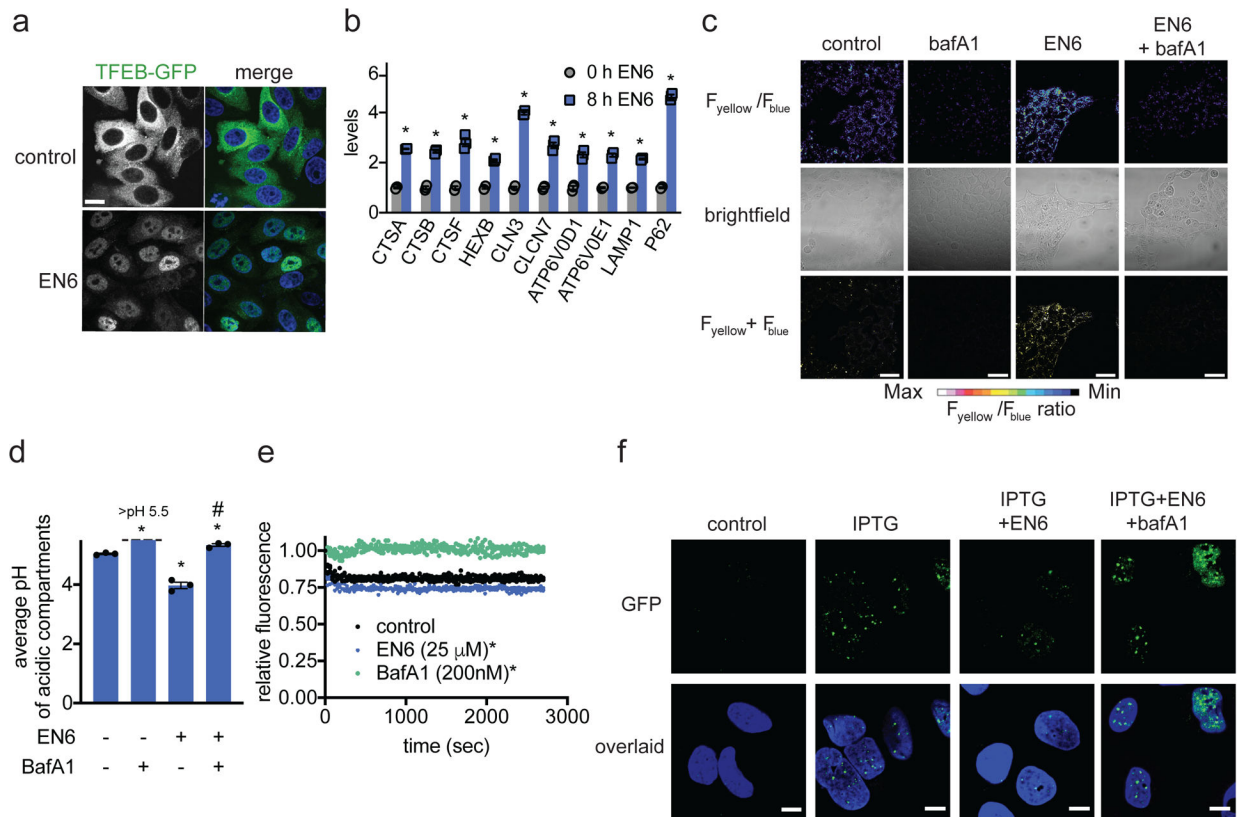


**Figure 4. EN6 effects on TFEB, lysosomal acidification, and clearance of TDP-43 aggregates.** **(a)** Localization of TFEB-GFP in HeLa cells treated with vehicle DMSO or EN6 (25  $\mu\text{M}$ , 4 h). Cells were stained with Hoechst 33342 (blue) and GFP-TFEB (green) were imaged by microscopy. Shown are representative microscopy images and quantification of percentage of nuclear TFEB from  $n=6$  and 7 biologically independent samples/group for vehicle-treated and EN6-treated groups, respectively. Scale bar in **(a)** denotes 10  $\mu\text{m}$ . **(b)** Gene expression of TFEB target genes in HeLa cells treated with EN6 (25  $\mu\text{M}$ ) for 0 or 8 h, assessed by qRT-PCR from  $n=3$  biologically independent samples/group. **(c)** Lysosomal acidification of HEK293A cells treated with vehicle DMSO, bafilomycin A1 (0.2  $\mu\text{M}$ ), EN6 (50  $\mu\text{M}$ ), or with co-treatment of EN6 and bafilomycin A1 for 4 h, readout by LysoSensor DND-160. Microscopy images shown in **(c)** are representative images from  $n=3$  biologically independent samples/group. Scale bar in **(c)** denotes 40  $\mu\text{m}$ . **(d)** Quantification of lysosomal acidification from experiment described in **(c)**, expressed as average pH of acidic compartments. pH calibration curve can be found in Supplementary Fig. 4d. **(e)** *In vitro* v-ATPase activity measurement. Organellar fraction containing lysosomes loaded with DxOG514 were isolated from HEK293T cells. Vehicle DMSO control, EN6 (25  $\mu\text{M}$ ), or BafA1 (200 nM) were added along with 5 mM ATP and  $\text{MgCl}_2$  were added at the start of the experiment and quenching of fluorescence emission over time was measured (see methods section for details). Data shown are from  $n=4$  biologically independent samples/group. **(f)** Effect of EN6 and bafilomycin treatment on TDP-43 aggregate clearance. U2OS cells expressing an IPTG-inducible GFP-TDP-43 were co-treated with vehicle DMSO, IPTG (50  $\mu\text{M}$ ), IPTG and EN6 (25  $\mu\text{M}$ ), or IPTG, EN6, and bafilomycin (0.2  $\mu\text{M}$ ) for 7 h. Cells

were stained with Hoechst 33342 (blue) and GFP-TDP-43 puncta (green) were imaged by confocal fluorescence microscopy in **(f)**. Microscopy images are representative images from  $n=26$  individual cells from 3 biologically independent samples/group. Scale bar in **(f)** denotes 10  $\mu\text{m}$ . Data shown in **(b, d, and e)** as average  $\pm$  sem. Statistical significance was calculated with unpaired two-tailed Student's t-tests for **(b, d)** and with a paired t-test of all data for each group in **(e)**. Significance is expressed as  $*p=8.0\times 10^{-7}$ ,  $4.0\times 10^{-5}$ ,  $4.4\times 10^{-4}$ ,  $3.0\times 10^{-3}$ ,  $1.9\times 10^{-6}$ ,  $1.5\times 10^{-4}$ ,  $4.6\times 10^{-4}$ ,  $4.7\times 10^{-5}$ ,  $1.7\times 10^{-6}$ ,  $1.4\times 10^{-6}$  for CTSA, CTSB, CTSF, HEXB, CLN3, CLCN7, ATP6V0D1, ATP6V0E1, LAMP1, P62, respectively, compared to 0 h control groups for **(b)**;  $*p=1.5\times 10^{-5}$ ,  $6.4\times 10^{-4}$ ,  $4.5\times 10^{-3}$  for BafA1, EN6, and BafA1/EN6 groups, respectively, compared to vehicle-treated control groups and  $\#p=3.1\times 10^{-4}$  compared to EN6-treated groups for **(d)**;  $*p<0.0001$  compared to vehicle-treated control groups in **(e)**.

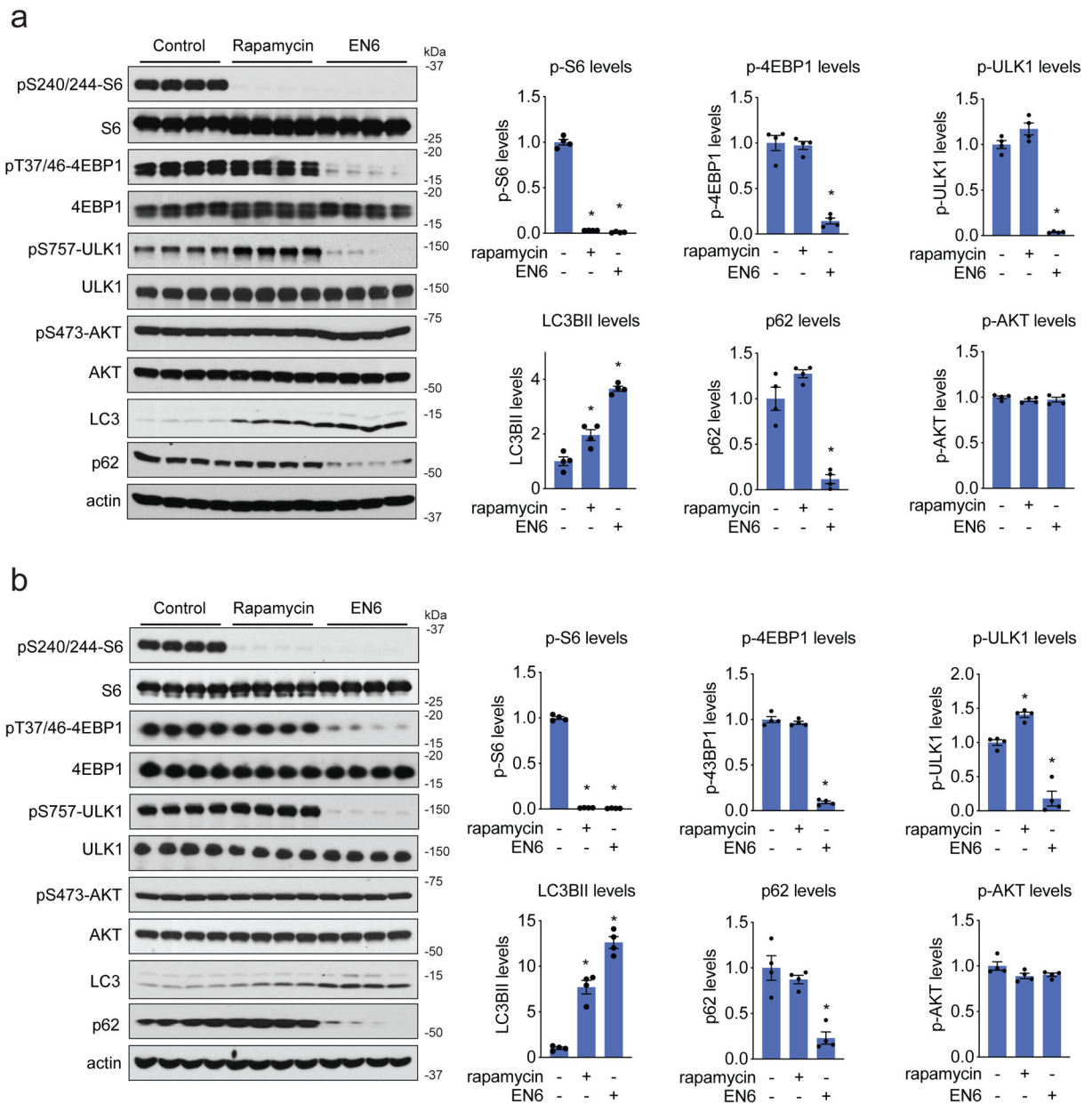


**Figure 5. EN6 inhibits mTORC1 signaling in mice.**

**(a, b)** mTORC1 signaling in mouse heart **(a)** and skeletal muscle **(b)**. C57BL/6 male mice were treated intraperitoneally with vehicle (18:1:1 saline:ethanol:PEG40), rapamycin (10 mg/kg) or EN6 (50 mg/kg) for 4 h. mTORC1 and AKT signaling and autophagy markers LC3B and p62 levels were measured by Western blotting and quantified by densitometry. LC3BII and p62 levels were normalized to actin loading controls. pS6, p4EBP1, pULK1, and pAKT were normalized to total S6, 4EBP1, ULK1, and AKT protein levels. Original gel images for **(a)** and **(b)** are in Supplementary Fig. 11a and 11b, respectively. All normalized values were then normalized to vehicle-treated control levels. Data shown are average  $\pm$  sem,  $n=4$  biologically independent animals/group. Statistical significance was calculated with unpaired two-tailed Student's *t*-tests. Significance is expressed compared to vehicle-

treated control groups as  $*p=7.3\times 10^{-8}$ ,  $6.6\times 10^{-8}$  in **(a)** and  $*p=1.0\times 10^{-9}$ ,  $1.0\times 10^{-9}$  in **(b)** for rapamycin and EN6 treatment groups, respectively, for p-S6 levels;  $*p=7.5\times 10^{-5}$  in **(a)**,  $2.5\times 10^{-7}$  in **(b)** for EN6 treatment groups for p-4EBP1 levels;  $*p=5.9\times 10^{-7}$  for EN6-treated groups in **(a)** and  $*p=3.6\times 10^{-4}$ ,  $4.1\times 10^{-4}$  for rapamycin and EN6-treated groups, respectively, in **(b)** for p-ULK1;  $*p=9.3\times 10^{-3}$ ,  $6.8\times 10^{-6}$  in **(a)** and  $*p=1.1\times 10^{-4}$ ,  $2.2\times 10^{-3}$  in **(b)** for rapamycin and EN6-treated groups, respectively, for LC3BII levels;  $*p=6.4\times 10^{-4}$ ,  $2.2\times 10^{-3}$  for **(a)** and **(b)**, respectively, for EN6-treated groups for p62 levels.

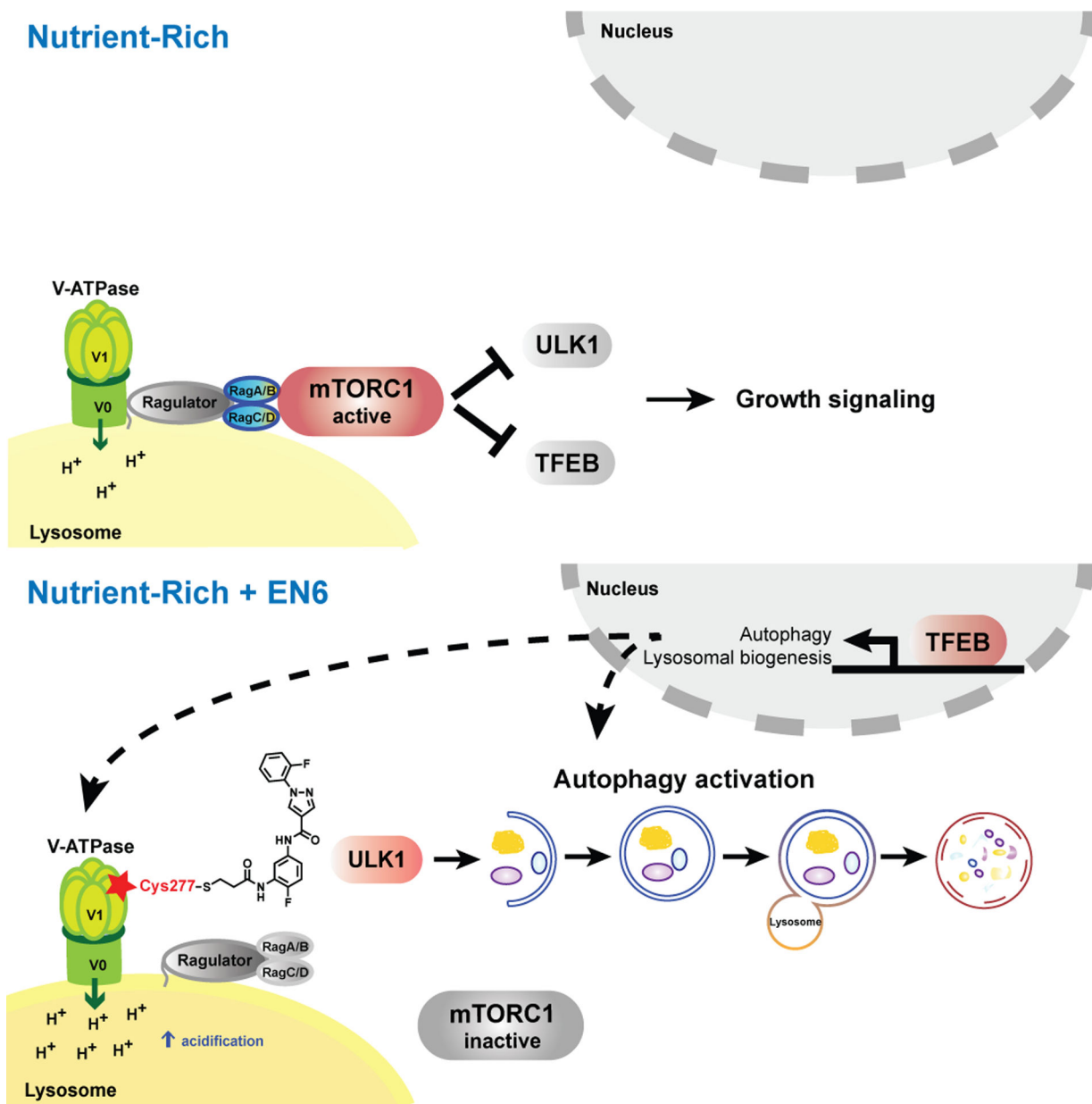


**Figure 6.** Scheme of v-ATPase-mTORC1 regulation of autophagy and mechanism of **EN6** action. (top) Under full nutrient conditions, the Ragulator-Rag GTPases recruit mTORC1 to the lysosomal surface, where mTORC1 kinase function is activated, leading to pro-growth signaling and suppression of autophagy via inhibitory phosphorylation of ULK1 and TFEB. The nutrient-induced switch of the Rag GTPases from the inactive to the active, mTORC1-binding state requires several upstream factors including the v-ATPase. (bottom) By covalently modifying Cys277 in the ATP-hydrolyzing domain of the v-ATPase, EN6 causes its physical and functional decoupling from the Ragulator-Rag GTPase complex. This leads to mTORC1 release to the cytoplasm and its inactivation, triggering autophagy initiation and transcriptional upregulation of autophagic-lysosomal biogenesis via TFEB. Additionally,



EN6-mediated modification boosts the rate of proton pumping by the v-ATPase, leading to increased acidification of the lysosomal lumen. Combined mTORC1 inhibition and v-ATPase stimulation by EN6 lead to increased cellular clearance.

Author Manuscript

Author Manuscript

Author Manuscript

Author Manuscript